NUMERICAL ANALYSIS OF ELECTRICAL FLUID AND ROCK RESISTIVITY IN HYDROTHERMAL SYSTEMS

by

Bruce Matthew Moskowitz

A Thesis Submitted to the Faculty of the

DEPARTMENT OF GEOSCIENCES

In Partial Fulfillment of the Requirements
For the Degree of

MASTER OF SCIENCE

In the Graduate College

THE UNIVERSITY OF ARIZONA

1 9 7 7

STATEMENT BY AUTHOR

This thesis has been submitted in partial fulfillment of requirements for an advanced degree at The University of Arizona and is deposited in the University Library to be made available to borrowers under rules of the Library.

Brief quotations from this thesis are allowable without special permission, provided that accurate acknowledgment of source is made. Requests for permission for extended quotation from or reproduction of this manuscript in whole or in part may be granted by the head of the major department or the Dean of the Graduate College when in his judgment the proposed use of the material is in the interests of scholarship. In all other instances, however, permission must be obtained from the author.

SIGNED: Bruce H. Tschourz

APPROVAL BY THESIS DIRECTOR

This thesis has been approved on the date shown below:

Robert F Butler

ROBERT F. BUTLER
Assistant Professor of Geosciences

4/28/77

Date

ACKNOWLEDGMENTS

I wish to sincerely thank Denis Norton and Robert Butler for their guidance and helpful suggestions throughout the writing of this thesis. I hope that my friendships with Denis and Bob, which generated from my graduate studies at Arizona, will continue through the coming years. Also, I wish to thank R. Knapp, J. Knight, and G. Beaudoin, as well as the rest of the irreversible gang at The University of Arizona, for many relevant and sometimes irrelevant discussions. Most of all, I wish to thank Mary Beth for her never-ending support. Finally, this study was supported by ERDA grant E111-2763 and all computing was done at The University of Arizona Computer Center.

TABLE OF CONTENTS

LIST OF ILLUSTRATIONS

LIST OF ILLUSTRATIONS--Continued

LIST OF ILLUSTRATIONS--Continued

LIST OF TABLES

ABSTRACT

Intrinsic rock resistivity, calculated by Archie's Law, has been numerically modeled as a function of space and time for two, two-dimensional crustal environments. The effects of variations in porosity and pore-fluid resistivity (with temperature and pressure) have been included in Archie's Law. The two crustal environments investigated are characterized by pluton emplacement within the upper 10 km of the crust. Both crustal models were numerically modeled from the time of pluton emplacement to 2×10^5 years after emplacement. The calculations indicate that the host-rock resistivity distribution is primarily controlled by the mode of dispersion of thermal energy away from the pluton. Comparisons between model results and field observations in geothermal areas indicate that (1) low near-surface resistivity cannot be entirely accounted for by hot circulating saline water, and (2) observations of high thermal gradients associated with low resistivity anomalies do not assure the existence of a high energy geothermal source at shallow crustal depths.

INTRODUCTION

The nature of the earth's upper crust has been the focus of many areas of research within the past decade. Data on the upper crust, ranging from gravity to geochemical surveys, have been collected, and analyses of these data are abundant in the scientific literature. The present study is exploratory in nature, aimed at achieving an understanding of the electrical properties of the earth's upper crust.

The electrical nature of the earth's crust has recently received much attention from two areas of research. The first is the possibility of a lithostatic electromagnetic wave guide, which is directly dependent on the existence of a continuous zone of highly resistant rocks within the crust (Heacock, 1971). The second area of research is directed toward the evaluation of low crustal resistivity as a diagnostic feature of geothermal areas. Although these research areas seem widely divergent, the causative agents affecting rock resistivity in both of these areas are the same: water content, porosity, temperature, mineralogy, and pore-fluid properties. The present study is an attempt, on the basis of computer modeling, to analyze the relationships between the variables which determine intrinsic resistivity in the upper 10 km of the crust. Implicit in these resistivity models is the modeling of thermally induced fluid circulation within the crust, as described in Norton and Knight (in press). Limitations imposed upon these computer models, due to insufficient data regarding permeability and total porosity, prohibit the resistivity models from precisely predicting the resistivity

structure in the subsurface. However, these models can provide a basis for establishing geologic bounds on crustal resistivity, as well as a focal point for future crustal studies.

Previous Work

The transient aspect of the evolution of host-rock resistivities around a thermal source within the crust has not been discussed in the literature. In order to simulate this resistivity distribution, the computation of thermal energy dispersion around a thermal source within the crust must first be accomplished. The most extensive numerical analysis of a cooling pluton within the crust is given by Norton and Knight (in press). The models presented in their study are used in the present investigation.

Observational data on crustal resistivities, which represent an instant in geologic time, can be divided into two types. The first type is the large-scale resistivity surveys, which effectively examine deep crustal and upper mantle resistivities. These studies are usually performed away from areas of active volcanism. The second type is the resistivity surveys which are used for exploration purposes in geothermal areas.

The most noteworthy large-scale surveys are those by Keller (1971); Keller, Anderson, and Pritchard (1966); Porath (1971); Jackson (1966); and Brace (1971). All the above surveys revealed a 10 to 15 km thick surface zone, where resistivity increased with depth. The surface zone was underlain by a zone in which resistivity decreased with depth.

This zone extended into the mantle. Keller et al. (1966) attempted to correlate resistivity zones with seismic zones, although no clear correlation was accomplished. Porath (1971) observed three distinct zones: (1) a surface zone consisting of moderately low resistivities due to the presence of pore fluids, (2) an intermediate zone where resistivity increased, probably due to the decrease in porosity and pore-fluid content, and (3) at mantle depths, resistivities once again decrease as semiconduction in silicate minerals becomes important. A comparison of three different heat flow regions in the United States by Brace (1971) also produced similar results. Typical values quoted in the literature for upper crustal resistivities range from 10^2-10^6 ohm-m (Brace, 1971).

There is a vast amount of information in the literature on resistivity surveys in geothermal areas. Most, if not all, resistivity surveys in geothermal areas reveal a well-defined correlation between hydrothermal alteration and low resistivity. Low resistivity layers of 3-20 ohm-m have been observed in numerous areas in Japan (Sato, 1970). The Tatum Volcanic region in Taiwan shows a low resistivity layer (15-20 ohm-m) which correlates with layers of high temperature and hydrothermal alteration (Cheng, 1970). Resistivity lows at depths of 100-250 m are observed at Broadlands, New Zealand (Risk, MacDonald, and Dawson, 1970). Results from resistivity surveys conducted at Yellowstone National Park also showed anomalously low near-surface resistivities (Zohdy, Anderson, and Muffler, 1973). At Yellowstone a fairly uniform layer of 2-6.5 ohm-m occurs at an average depth of 50 feet and extends to approximately 250 feet. Zohdy et al. attribute the low resistivity values to hot water and to the presence of pyrite and clay minerals.

It is apparent from the observational data that geothermal areas are characterized by near-surface low resistivity (<50 ohm-m), as a result of circulating hot fluids and conductive minerals. On the other hand, areas between active centers of volcanism are characterized by near-surface values ranging between 10^2-10^6 ohm-m.

Objectives, Scope, and Methodology

Heretofore no known study on the transient nature of intrinsic resistivity of host rocks around a cooling pluton has been attempted. This investigation is concerned with the following question: Given a set of geologic initial conditions, what is the evolution of host-rock resistivity around a thermal source with time and space, and is this thermally-induced resistivity distribution consistent with field observations? The method of analysis of this problem is through the use of computer simulation of geologic processes involved in the thermal decay of a pluton within the upper crust. The computer models afford for variations in permeability and porosity, heat sources, rock and fluid properties, including variation in pore-fluid resistivity as a function of temperature, pressure, and concentration, as well as the time dependence of these models in a two-dimensional domain. Coupled with the numerical approximations of the governing equations (Norton and Knight, in press), an interactive graphics system has been developed in order to present the model results in a coherent fashion. The interactive graphics system allows a user to time step through a given model, stopping at specified times to analyze the steady-state solutions of the governing equations.

Combining the numerical approximation techniques and the interactive graphics system, two heuristic models will be analyzed in order to compute the evolution of host-rock resistivities with time. The processes contributing to dispersion of thermal energy away from a pluton with time are the major contributors to the distribution of host-rock resistivity. Comparisons of these models with active geothermal areas and with crustal sections between active areas of volcanism are the primary goals of this research endeavor.

ELECTRICAL CONDUCTION IN ROCKS

The purpose of this chapter is to review the basic principles of electrical conduction in rocks, and to review the experimental and theoretical data in the literature relating to the electrical phenomena in rocks. This is not intended to be a comprehensive study of the electrical conduction process. However, this chapter will cover most of the important parameters involved in the understanding of electrical conduction of crustal rocks. An adequate understanding of the parameters involved in the conduction process is needed before resistivity modeling of the crust is attempted and the results of these models properly interpreted.

Physical Principles

Before embarking on a general discussion of the electrical phenomena in rocks, the basic definitions of resistivity, conductivity, and types of electrical conductors will be presented.

The conductivity of a material is defined through Ohm's Law, which states

$$\overline{J} = \sigma \overline{E} \tag{1}$$

where: $\overline{J}$ = current density measured in amp/m^3

$\overline{E}$ = electric field strength measured in volt/m, and

σ = electrical conductivity measured in $ohm^{-1}m^{-1}$.

In isotropic materials, σ is independent of $\overline{E}$ and is constant for a given temperature and pressure.

Suppose that we consider a conducting rod of length, ℓ, and cross sectional area, A. The current density through the rod is simply

$$\overline{J} = \overline{I}/A = \sigma\overline{E} \tag{2}$$

where $\overline{I}$ is the current. Let V be the potential difference across the rod so that $E = V/\ell$, and equation (2) becomes

$$I = \frac{\sigma A}{\ell} V. \tag{3}$$

The resistance, R, for any given section of rod is given by $R = V/I$. Substituting the expression for R into equation (3), we may write the resistance of the rod as

$$R = \frac{\ell}{\sigma A}. \tag{4}$$

The resistivity, ρ, is defined as the inverse of σ, or

$$\rho = RA/\ell. \tag{5}$$

The resistivity of a material is thus measured in ohm-m. In isotropic materials, ρ and σ are reciprocals. However, on a microscopic scale, a basic physical difference exists. The conductivity is the flow mobility of charged particles, whereas the resistivity is the opposition to flow of charged particles.

Electrical Conductivity in Solids

Electrical conductors may be divided into three broad categories: (1) metallic, (2) electronic semiconductors, and (3) solid electrolytes. The high conductivity associated with metals results from the larger number of mobile electrons and the relatively small amount of energy required to move electrons from one atom to another. Imperfections in the crystalline structure of metals hinders the movement of electrons and, thereby, causes a decrease in conductivity. Also interfering with electron mobility are the thermal vibrations of metallic ions. These thermal vibrations result in a negative temperature coefficient of conductivity. Metallic conductors are usually characterized by conductivities $> 10^2$ $ohm^{-1}m^{-1}$ (at $T = 0^oC$).

Conduction in semiconductors is also by electron motion, but due to a decrease in mobile electrons, conductivity is much lower than in metallic conductors. Thermal agitation results in an increased free electron density and yields an increase in conductivity. Semiconductors are characterized by a positive temperature coefficient of conductivity for at least part of the temperature scale. Semiconductors usually have conductivities which range between 10^{-2}-10^{-8} $ohm^{-1}m^{-1}$.

The major difference between solid electrolytes and the preceding types of conductors is that conduction in electrolytes is due to the movement of ions. Inherent imperfections in solid electrolytic crystalline structures (viz. holes) cause a small number of vacancies to be present throughout the lattice. As thermal energy increases, ions have a tendency to "jump" into available vacancies at random. When an

electric field is applied to the lattice, the electric field exerts a bias to the random jumping of ions into vacancies, which constitutes the current flow. Solid electrolytes have conductivities < 10^{-8} $ohm^{-1}m^{-1}$.

Examples of metallic conductors in nature are native metals, such as gold and silver. Sulfide ore minerals usually fall into the category of semiconductors, while most rock-forming minerals are solid electrolytes.

Water Resistivity

The pervasiveness of a stable fluid phase within the upper crust has received support from many areas of research. Observational data on crustal seismic velocities (Landisman, Mueller, and Mitchell, 1971; Mitchell and Landisman, 1971) and continental resistivity surveys (Keller, 1971; Porath, 1971; Jackson, 1966) correlate well with laboratory seismic velocity and resistivity data on fluid-saturated crustal rocks (Simmons and Nur, 1968, 1969; Brace, 1971; Brace, Orange, and Madden, 1965; Brace and Orange, 1968a, 1968b). Results from computer simulation of pluton intrusion into the crust indicate that large areas of the crust might be characterized by thermally-driven fluid circulation (Norton and Knight, in press). World-wide occurrences of geothermal areas also indicate an abundance of fluid water at depth.

Table 1 shows average fluid resistivity data for a broad range of geologic environments. The range of values is from .061 ohm-m to 11.0 ohm-m. It is evident from these data that water resistivity is many orders of magnitude lower than resistivities for many rock-forming minerals. As a consequence of the low resistivity of water, the electrical

Table 1. Average Values of Connate Water Resistivity.

Geologic Environment	Average Resistivity (ohm-m)[1]
Igneous rocks, Europe	7.6
Igneous rocks, South Africa	11.0
Metamorphic rocks, South Africa	7.6
Metamorphic rocks, Australian Precambrian	3.6
Pleistocene to Recent Sedimentary rocks from Europe	3.9
Pleistocene to Recent Sedimentary rocks from Australia	3.2
Tertiary Sedimentary rocks from Europe	1.4
Tertiary Sedimentary rocks from Australia	3.2
Mesozoic Sedimentary rocks from Europe	2.5
Paleozoic Sedimentary rocks from Europe	.93
Chloride waters from oil fields	1.2
Bicarbonate waters from oil fields	.98
Morrison Formation (Jurassic), Colorado-Utah	1.8
Cisco Series, North Texas	.061
Des Moines Series (Pennsylvanian), Central Oklahoma	.062

[1]Taken from Keller and Frischknecht (1966).

conductivity of the upper crust might be dominated by the fluid phase rather than by conduction through mineral grains themselves. For this reason, the composition and distribution of subsurface solutions for the temperatures and pressures prevailing in the upper crust must be investigated in order to adequately understand crustal resistivity.

The most extensive experimental work on the electrical conductivity of aqueous electrolytic solutions was published by Quist, Franck, Jolley, and Marshall (1963), and Quist and Marshall (1968, 1969). Previous to this, Gunning and Gordon (1942) and Chambers (1958) tabulated data concerning the behavior of NaCl and KCl solutions. For reasons to be explained later, only data covering NaCl solutions collated from the above sources will be used in the present study. The data on NaCl solutions span the temperature range of 25°C to 675°C and the pressure range 1 bar to 1000 bars.

Conduction in an aqueous electrolyte is a consequence of aqueous ion mobilities. The conductance is simply the sum of the different ionic mobilities present in the solution. In equation form, the conductance, Λ, is

$$\Lambda = \sum_{i}^{n} e_i \mu_i n_i, \tag{6}$$

where: μ_i = mobility of i^{th} ion,

n_i = number of i^{th} ions, and

e_i = charge of i^{th} ion.

The mobility of various ions present in subsurface fluids at 25°C is on the order of $10^{-8} m^2/sec\text{-}v$ (Keller and Frischknecht, 1966).

Figure 1 shows the resistivity of various salt solutions as a function of concentration. One can clearly see the close grouping of the various salts, owing to the similar ionic mobilities. Geochemical analysis of subsurface waters, especially in geothermal areas, indicates a predominance of Na^+ and Cl^- ions (Lindal, 1970; Wong, 1970; Kramer, 1969; White, 1964). It is a reasonable simplification to use NaCl solutions instead of a more representative sample for subsurface waters for two reasons:

1) They usually contain five to ten times more Na^+ and Cl^- ions than other constituents.
2) The resistivity of the different salt solutions at constant concentration does not vary by more than a few percent.

Figure 2 shows the effect of temperature and pressure on the resistivity of a .01 molal NaCl solution. Resistivity is seen to decrease almost independent of pressure until approximately 300°C. The dominant pressure effect is to shift the resistivity minimum to higher temperatures with increasing pressure. In order to understand this behavior, the physical properties of the H_2O system must first be investigated, specifically, viscosity, density, and dielectric constant.

The principle mode of conduction in aqueous solutions is through the movement of ions. At constant concentration, as solvent viscosity decreases, the ions are freer to move, therefore decreasing resistivity.

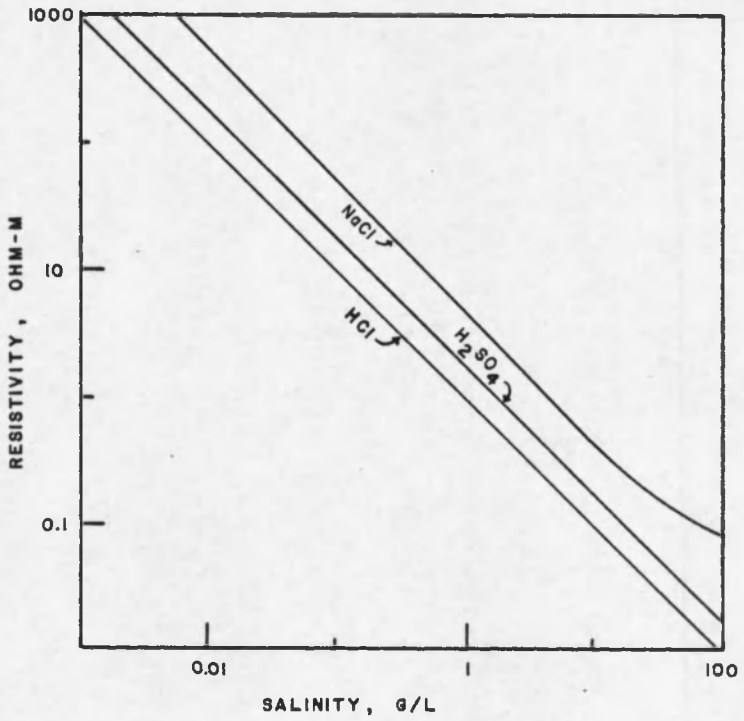

Figure 1. Relationship between Resistivity and Concentration for various Salt Solutions at a Temperature of 18°C (Keller, Anderson, and Pritchard, 1966).

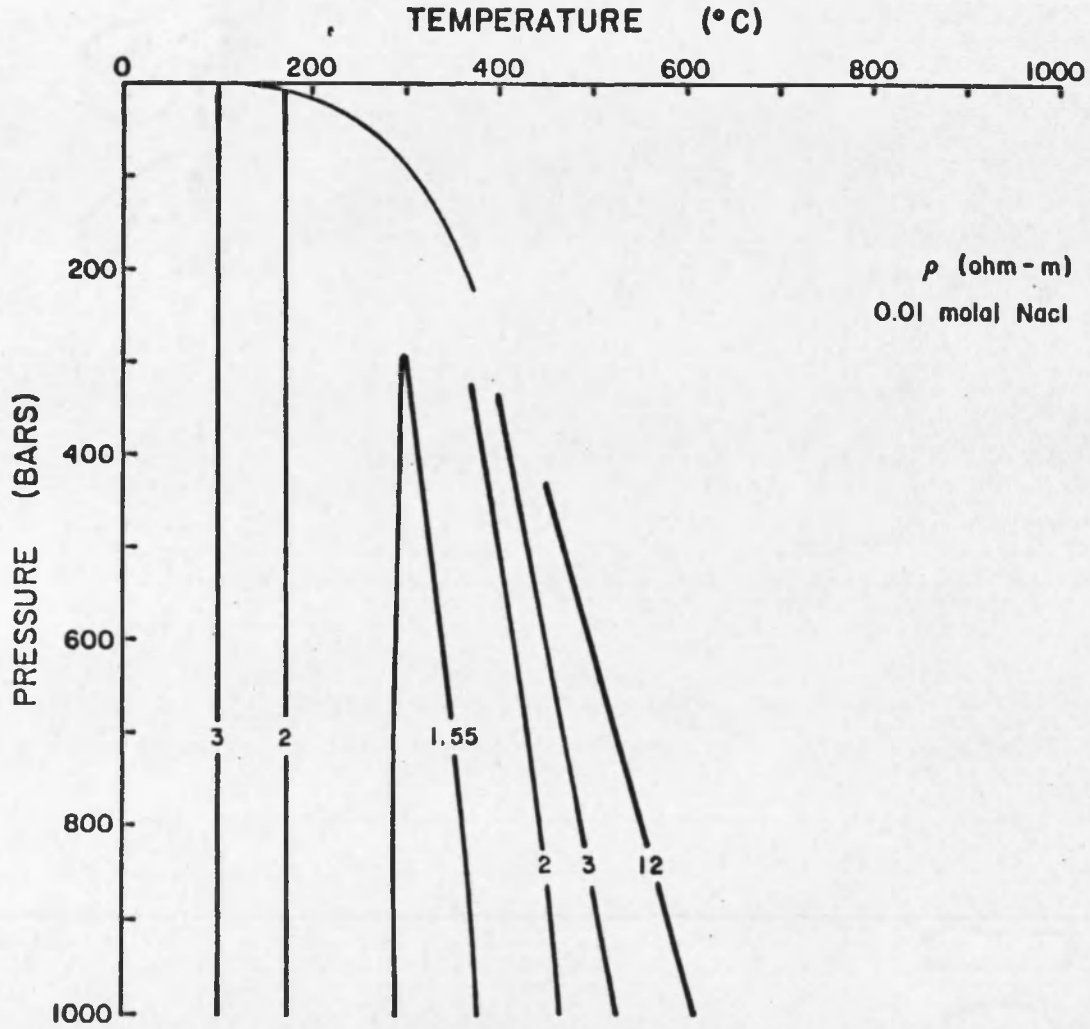

Figure 2. Resistivity of .01 Molal NaCl Solution as a Function of Temperature and Pressure. -- Unlabeled curve represents the two-phase surface (liquid-vapor) in the H_2O system.

Decreasing solvent density causes an increase in resistivity due to the reduction in ions per unit volume. The dielectric constant, which determines the force of attraction between two charged particles, also plays a dominant role in the resistivity of water. A low dielectric constant results in a stronger electrostatic force between charged particles, promoting less dissociation into ions. Figure 3 shows viscosity, density, and dielectric constant as a function of temperature at a pressure of 500 bars. It is evident from these data that the rapid decrease in viscosity with increasing temperature is the dominant cause for the initial decrease in resistivity to 300°C. Above 300°C, the density decrease, coupled with the lowering of the dielectric constant, counteracts the viscosity effect and causes the resistivity to increase. Figure 4 shows the effect of increased concentration. As expected, resistivity is directly related to concentration, owing to the variation in ion density (Quist and Marshall, 1968).

Referring to Figure 2 again, between 0°C and 200°C, the resistivity of water decreases by more than a factor of 5. This resistivity decrease will result in a low resistivity layer due to water between the 200°C and 300°C isotherms in the crust. In active geothermal systems, temperatures between 200°C and 300°C are present within a kilometer of the surface (Sato, 1970; Grindley, 1970; Smith, 1970). In normal geologic environments, the 200°C isotherm might not be reached until depths of 6 km (Brace, 1971). Therefore, in active geothermal systems, a decrease in resistivity due to hot water might cause anomalously low near-surface resistivity.

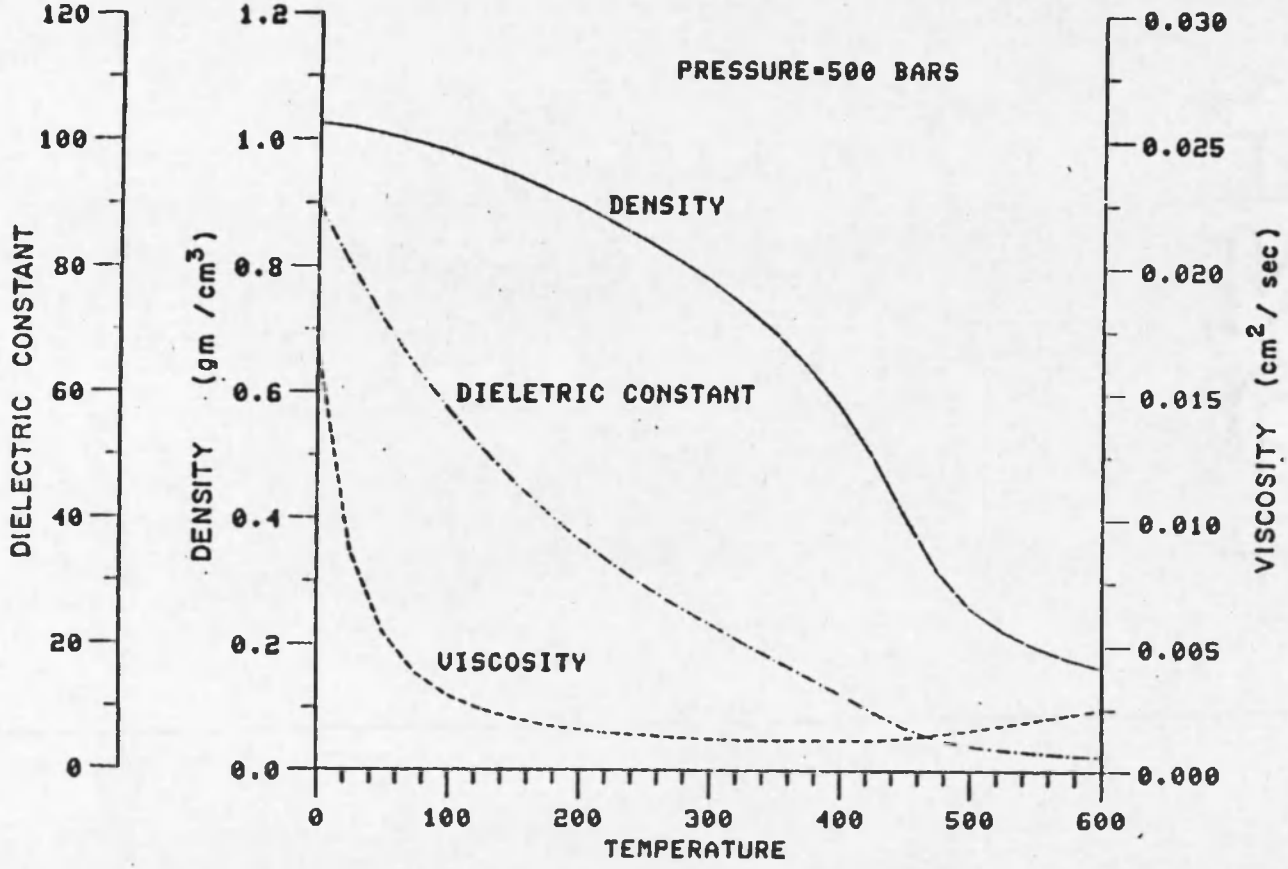

Figure 3. Density, Viscosity, and Dielectric Constant of Pure Water as a Function of Temperature and at Pressure of 500 Bars.

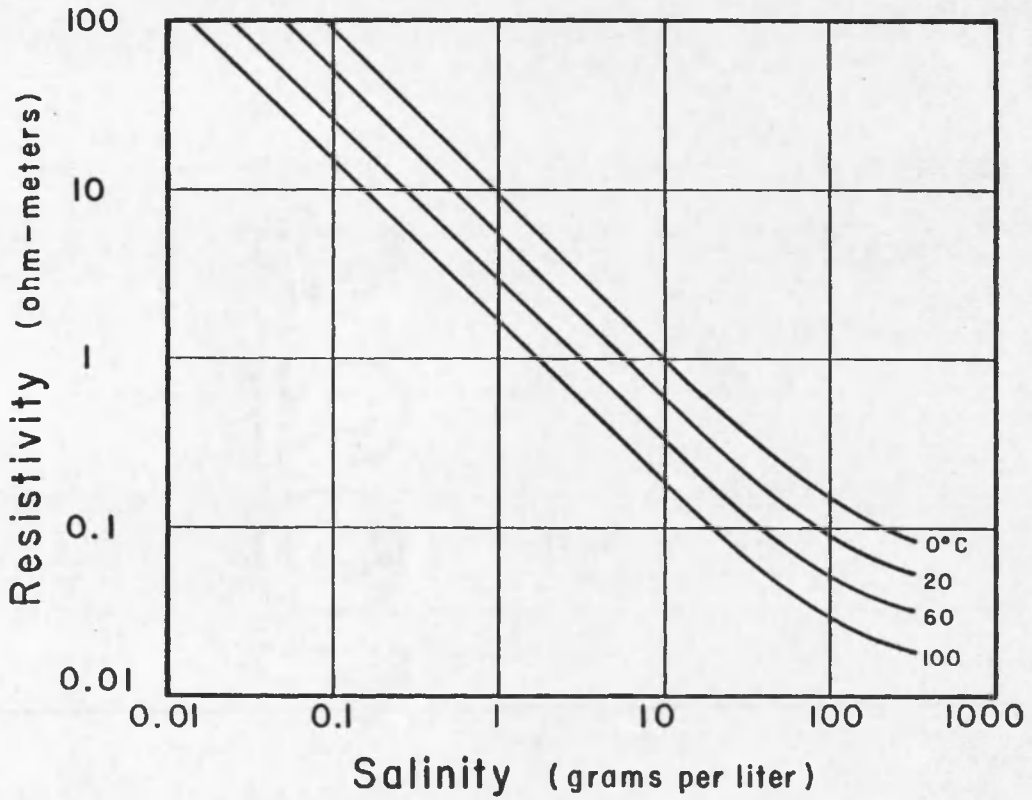

Figure 4. Resistivity of Solutions of Sodium Chloride as a Function of Concentration and Temperature (Keller, Anderson, and Pritchard, 1966).

Rock Resistivity

The factors which directly affect the intrinsic resistivities of crustal rocks are:

1) fluid content,
2) porosity,
3) salinity,
4) temperature,
5) pressure,
6) mineral conduction, and
7) clay content.

The first five factors listed above are the most important parameters which influence average crustal resistivities, whereas the last two (mineral conduction and clay content) might become dominant in special geologic environments. In the previous section the resistivity of water was discussed, and porosity will be discussed in the next chapter. Most of the data concerning temperature and pressure effects on rock resistivities are derived from laboratory measurements. Mineral conduction and clay content will also be briefly reviewed.

Experimental determinations of resistivities over a wide range of crustal rock types has been published by Brace, Walsh, and Frangos, 1968; Brace et al., 1965; Brace and Orange, 1968a, 1968b; and Parkhomenko, 1967. Dry rock resistivities are usually on the order of 10^8-10^9 ohm-m. However, when saturated with saline water, these same rocks exhibit resistivities which are three to four orders of magnitude lower (Keller, 1971; Brace et al., 1965). Dry rock conduction will not become important

until lower crust and upper mantle depths are attained (Keller, 1971; Brace, 1971). Studies on saturated rocks are, therefore, of prime importance, especially when one considers geothermal areas where large volume of fluid might be present.

Increased temperatures will produce a lowering of bulk rock resistivities in saturated rocks (Brace, 1971). This decrease in resistivity is due to the behavior of the pore fluids (see previous section). As lower crustal temperatures are reached, where fluids are apparently not present, semiconduction in minerals becomes important in lowering resistivity. The pressure effect is more complicated, resulting from the closure of conduction pathways. Figures 5 and 6 show the effect of temperature and pressure on typical crystalline rock resistivities.

In general, increasing hydrostatic confining pressure yields increased resistivity due to the closure of cracks. According to Brace (1971), cracking induced by thermal expansion of pore fluids is negligible as long as pressure and temperature increase together. However, in typical geothermal areas, the intrusion of a hot igneous body into the upper crust will cause a high temperature anomaly to propagate toward the surface (Norton and Knight, in press). In this case, temperature increases while confining pressure remains constant, and the thermal stresses due to pore-fluid expansion must be taken into consideration (Knapp and Knight, in prep.).

The presence of conducting minerals, such as pyrite, pyrrhotite, and graphite will appreciably alter the electrical nature of a rock. Keller (1971) points out that the presence of conductive minerals might

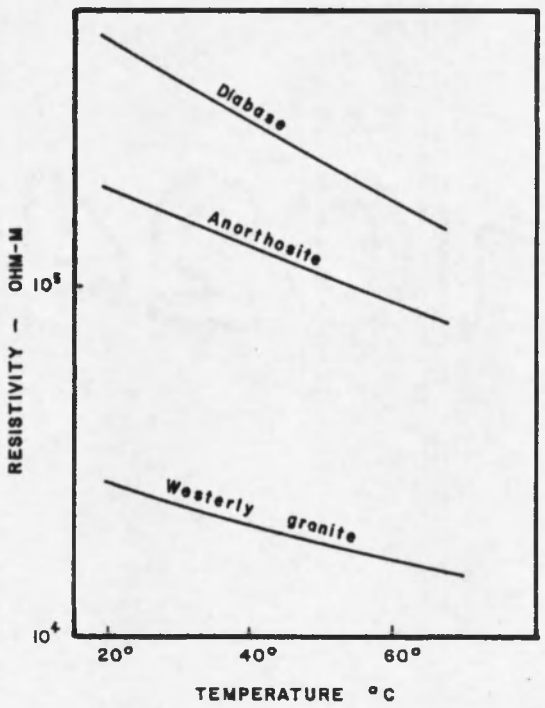

Figure 5. Resistivity of Some Crystalline Rocks as a Function of Temperature (Brace and Orange, 1968b).

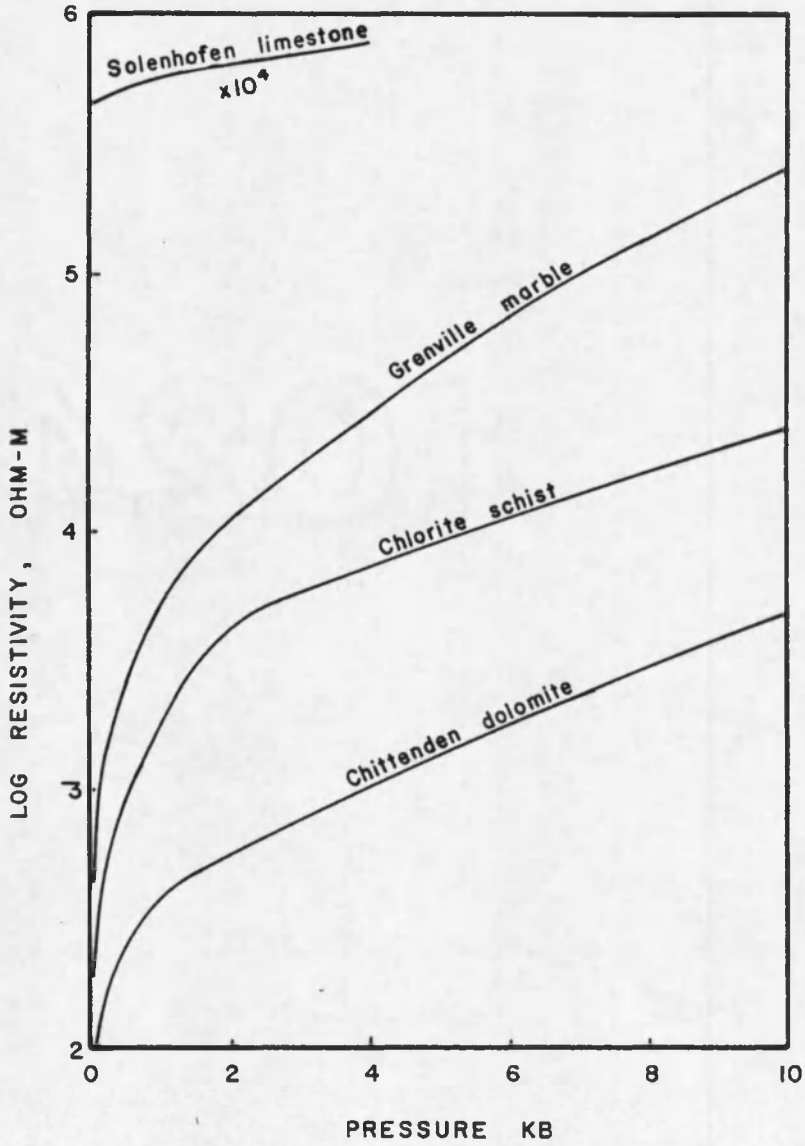

Figure 6. Resistivity of Some Crystalline Rocks Saturated with Salt Solutions as a Function of Pressure at a Temperature of 20°C (Brace and Orange, 1968b).

reduce a rock's resistivity by more than three orders of magnitude. Keller also points out that the distribution of conducting minerals is an important parameter. Disseminated or vein type deposits might have a negligible influence on the intrinsic resistivity of a rock, due to the discontinuous pathways of the conducting minerals. Pyrite and other sulfide minerals have been found in many geothermal systems in varying amounts (Browne and Ellis, 1970; Zohdy et al., 1973). The influence of these conducting minerals may have a profound influence on the intrinsic resistivities, and must be taken into account before any adequate interpretation of crustal resistivity is presented.

The amount of clay content in the pore structure of rocks will also tend to decrease resistivity through the mechanism of cation exchange capacity. Cation exchange capacity is a process which adds ions to the normal ionic concentration in a fluid-filled pore. All minerals exhibit cation exchange capacity, but such minerals as kaolinite, montmorillonite, and chlorite have significant exchange capacities (Keller, 1971). Cation exchange capacity occurs due to an electrical charge imbalance in the crystal of a clay mineral. Cations are absorbed from solution to attain electrical neutrality. However, the finite size of the absorbed cations results in the formation of a double layer of cations on the crystalline surface of the clay mineral. The fixed layer forms adjacent to the crystalline surface. In the second layer (diffuse layer) ions are mobile and, thus, contribute more ions to the normal ionic concentration in the pore fluid. In very dilute saline solutions cation exchange capacity will contribute a significant increase in electrical

conduction. However, increasing the salinity of the pore fluid will result in a lessening influence of exchange capacities of clay minerals (Ward and Fraser, 1967). Clay minerals are also present in geothermal areas (Browne and Ellis, 1970; Zohdy et al., 1973), and their influence should not be overlooked.

In summary, the bulk rock resistivity may be evaluated from the following empirical relationship

$$\rho_R = f(T,P,\phi,C_{ex},C_m,s,\rho_w) \tag{7}$$

where: T = temperature,

P = pressure,

ϕ = porosity,

C_{ex} = cation exchange capacity,

C_m = conducting minerals,

s = salinity, and

ρ_w = water resistivity.

In the models presented in this study, ρ_R is seen to vary according to $f(T,P,\phi,\rho_w,s)$. The influence of conducting minerals (C_m) and clay minerals (C_{ex}) can only be inferred from discrepancies between model results and observation.

Archie's Law

An empirical relationship known as Archie's Law relates the bulk-rock resistivity to pore-fluid resistivity (Archie, 1942). The relationship is

$$\rho_R = a\rho_w\phi^{-m} \tag{8}$$

where: ρ_R = bulk-rock resistivity,

ρ_w = pore-fluid resistivity

ϕ = porosity,

m = cementation factor, and

a = fit parameter.

Values for m vary between 1.3 for loosely consolidated materials to 2.2 for well cemented rocks (Keller, 1971). Brace and Orange (1968a, 1968b) obtained m = 2.0 for crystalline rocks, and this value is used in this study. The parameter, a, is close to unity and is used to fit a group of data to equation (8). In this study, a is taken as 1. When the relationships of the previous section are incorporated, equation (8) may be written as

$$\rho_R = \frac{\rho_{w(T,P,s)}}{\phi^2(T)} \tag{9}$$

wherein ρ_R now varies with temperature, pressure, and silinity while porosity, ϕ, varies with temperature.

A theoretical treatment of Archie's Law has also been attempted by analysis of electrical network models (Greenberg and Brace, 1969; Shankland and Waff, 1974). The results agree quite well with experimental data, resulting in a value of 2 for the cementation factor, m.

POROSITY

The proportionality constant which relates the pore-fluid resistivity to the intrinsic rock resistivity in Archie's Law is normally taken as the total porosity of the rock. The distribution of porosity in space and time is of prime importance in modeling the resistivity of crustal rocks. The purpose of this chapter is to discuss the nature of porosity and its variation in pluton environments as a function of temperature and time.

Total Porosity

The total porosity of a rock is defined as the ratio of pore volume to total rock volume. Nearly all rocks have some porosity, although the range in porosity is extremely broad. Some sedimentary and volcanic rocks have total porosities from 10 to 50%, while some crystalline rocks have total porosities <1% (Walsh and Brace, 1966). Using the formulation of Norton and Knapp (in prep.), total porosity, ϕ_T, may be represented as

$$\phi_T = \phi_F + \phi_D + \phi_R \tag{10}$$

where ϕ_F is flow porosity represented by through-going cracks and fractures. Diffusion porosity, ϕ_D, is represented by less continuous and more tortuous pathways. Residual porosity, ϕ_R, is represented by discontinuous, isolated pores.

Through-going cracks and fractures which constitute flow porosity are directly related to rock permeability.[1] A first order approximation analyzed by Norton and Knapp (in prep.) for rock permeability, k, is

$$k = \frac{nd^3}{12} \tag{11}$$

where n is the number of parallel fractures per unit length and d is the aperture size of a single fracture. Flow porosity is defined as the product of the number of parallel fractures and the aperture size

$$\phi_F = nd \tag{12}$$

Substitution of equation (12) into equation (11) yields the following relationship between flow porosity and permeability

$$k = \frac{\phi_F d^2}{12} \tag{13}$$

The maximum range in ϕ_F is from 10^{-2} to 5×10^{-8} (Norton and Knapp, in prep.).

Diffusion porosity is defined by pores in which the transport of aqueous components by fluid flow is insignificant with respect to diffusional transport. Diffusion pores would consist of small aperture and discontinuous fractures, usually bounded by flow porosity channels. Experimental observations show ϕ_D on the order of 10^{-3}-10^{-4} (Norton and Knapp, in prep.).

---

1. Rock permeability refers to permeability to fluid flow, and this definition is used throughout this study.

It is apparent from the preceding discussion that flow and diffusion porosity represent a small fraction of the total porosity observed in fractured media at surface conductions. The remaining fraction of total porosity is in the form of residual porosity. Residual porosity apparently accounts for more than 90% of the total porosity observed (Norton and Knapp, in prep.).

Porosity and Resistivity

Archie's Law is an empirical relationship. Inconsistencies in this law exist when attempting to correlate porosity to electrical conduction pathways in a quantitative way. The concept of total porosity as the sum of ϕ_F, ϕ_D, and ϕ_R and the relationships these porosity types have to conduction pathways will be used for the analysis of the inconsistencies. The focal point of this analysis is a thought experiment in which a rock is considered as an electrical circuit and the porosity types are equated to circuit elements.

The use of total porosity, ϕ_T in Archie's Law, seems to be an oversimplification; therefore, it would be useful to determine the effect which each individual type of porosity has on the electrical resistance of a rock. Each porosity type, in essence, contributes a different type of pathway for fluid flow or electrical current. A rock to which an electric current is applied may be thought of as an electrical circuit. The three porosity types offer a different amount of resistance to the electric current flow. Therefore, ϕ_F, ϕ_D, and ϕ_R may be equated to electrical circuit elements. Flow and diffusion porosity contain

interconnected passageways which traverse the rock. ϕ_F and ϕ_D may be considered resistors of varying resistance. Residual porosity, ϕ_R, owing to its discontinuous nature within a rock, should allow no current flow and can be modeled as an open switch. Figure 7 shows the circuit model of porosity. Applying these concepts to equation (9), Archie's Law may be rewritten with the substitution of equation (10) for ϕ_T as

$$\rho_R = \frac{\rho_w}{(\phi_R + \phi_F + \phi_D)^2} \tag{14}$$

Three limiting cases of equation (14) may be defined as

1) Flow resistivity: $\rho w/\phi_F^2$ $(\phi_D = \phi_R = 0)$

2) Diffusion resistivity: $\rho w/\phi_D^2$ $(\phi_F = \phi_R = 0)$

3) Residual resistivity: $\rho w/\phi_R^2$ $(\phi_F = \phi_D = 0)$.

The total bulk-rock resistivity, P_R, is not a simple summation of the above three cases. This analysis of porosity type and resistivity is simply being used to set some limits on P_R, when a rock contains only one type of pore structure. Table 2 gives the minimum and maximum values for P_R, given appropriate bounds on ϕ_F, ϕ_D, and ϕ_R. Flow and diffusion porosity are shown to produce high bulk-rock resistivity, while residual porosity results in low bulk-rock resistivity. Brace and Orange (1968a) have measured P_R on a number of crystalline rock types as a function of pressure. Brace's results indicate values for P_R on the order of 10^2-10^5 ohm-m at a pressure of 400 bars and a temperature of 20°C. Brace's values for P_R are on the same order as "residual resistivity" in

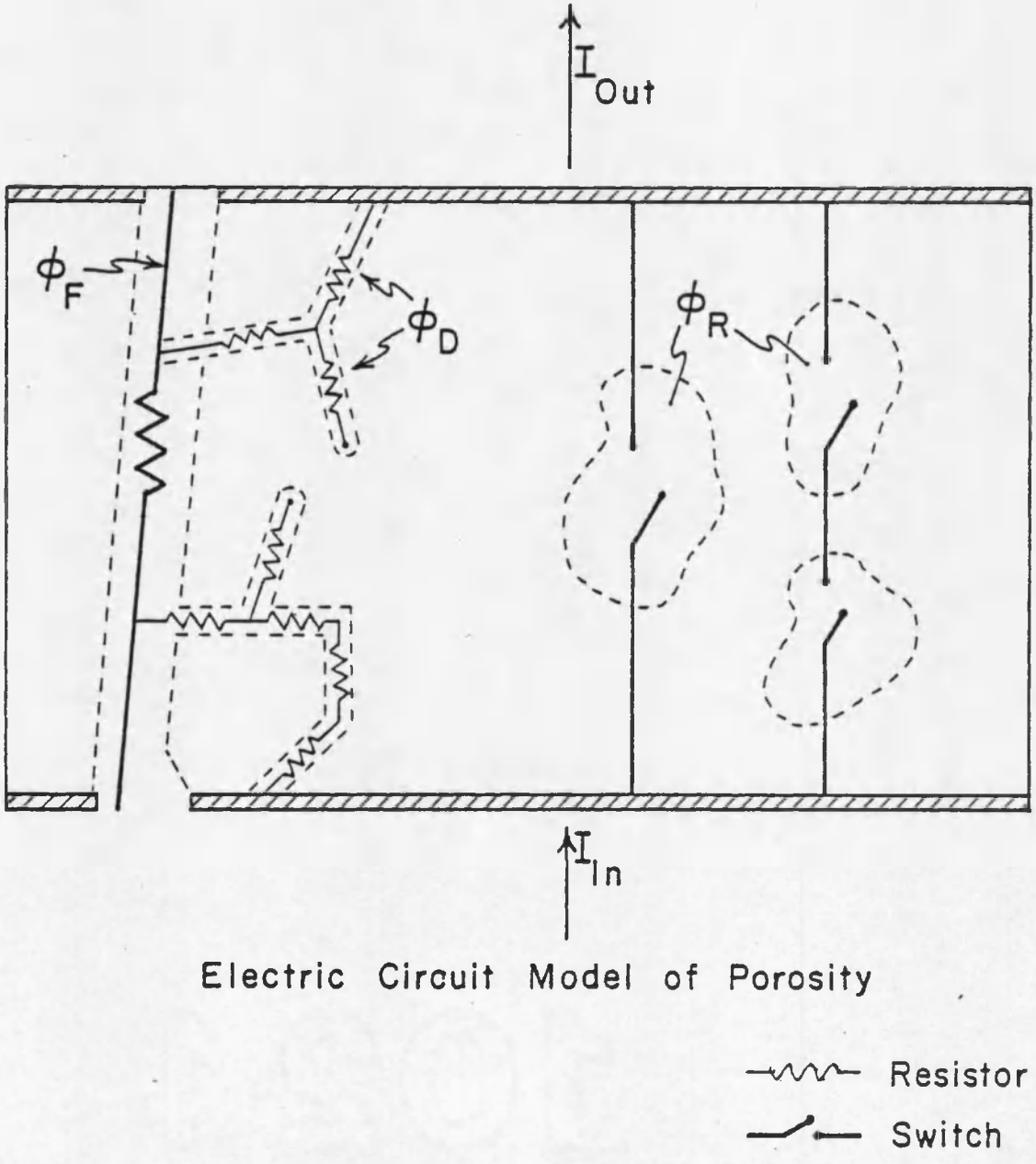

Figure 7. Electrical Circuit Model of Porosity. -- ϕ_F, ϕ_D, and ϕ_R are flow, diffusion, and residual porosity, respectively.

Table 2. Minimum and Maximum Values of ρ_R.

Porosity Type	Maximum Porosity[a]	Minimum Porosity	ρ_R[b] Minimum (ohm-m)	ρ_R Maximum (ohm-m)
ϕ_F	10^{-2}	5×10^{-8}	8.33×10^{3}	3.33×10^{14}
ϕ_D	10^{-3}	10^{-4}	8.33×10^{5}	8.33×10^{7}
ϕ_R	.45	.009	4.11	1.028×10^{4}
ϕ_T	.5	.01	3.33	8.33×10^{3}

[a]Porosity values taken from Norton and Knapp (in prep.).
[b]Values for ρ_R were determined using Archie's Law where

ρ_w = .833 ohm-m at

T = 20°C and P = 400 bars

Table 2. The data presented in Table 2 would indicate that ϕ_R is the dominant contributor to bulk-rock resistivity. However, residual porosity is modeled as an open circuit, while flow and diffusion porosity are modeled as resistors. If residual porosity is the dominant contributor to electric current flow, this model would indicate that more current flows through open circuits (ϕ_R) than through resistors of finite resistance (ϕ_F and ϕ_D). Since this is a logical contradiction, a fundamental question arises as to whether the actual quantity measured as porosity is the same quantity which controls electrical current flow. For example, the two schematic diagrams in Figure 8 might represent two hypothetical cases in rock porosity. In Figure 8a, total rock porosity is very high, due to the high residual porosity. Current flow in this rock would be confined to ϕ_F. The rock in Figure 8b exhibits very low total porosity, but flow and diffusion porosity are greater than in Figure 8a. Current flow in case (b) should be greater than in case (a) due to the increase in ϕ_F and ϕ_D, and, therefore, case (b) should have a lower resistivity. According to Archie's Law, case (a) would have the lower resistivity. This implies that current can flow more freely through the rock structure in case (a) than in case (b). This example illustrates that the theoretical basis of Archie's Law is not presently understood. Porosity must surely be related to electrical current flow. However, the effective electrical porosity for rocks has yet to be discovered.

Porosity Model

The horizontal and vertical distribution of porosity in the crust with space and time is a poorly known quantity. The effect of pressure

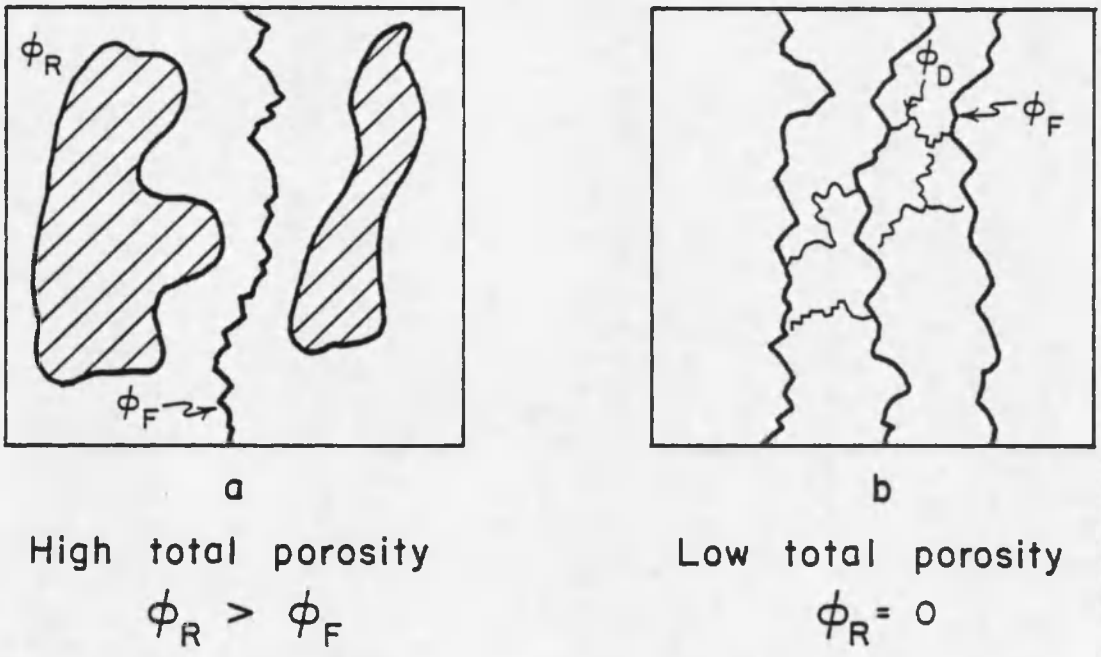

Figure 8. Hypothetical Examples of Distribution of ϕ_F, ϕ_D, and ϕ_R within a Rock.

on porosity is indirectly determined from laboratory measurements on crystalline rock resistivities (Brace et al., 1965; Brace and Orange, 1968a, 1968b; Brace et al., 1968; Brace, 1971). The temperature variation of porosity is not found in the literature. Brace (1971) assumes that thermal stresses associated with residual pore-fluid expansion are negligible as long as confining pressure is increasing at a greater rate than thermal expansion. However, Brace fails to define the geothermal gradients at which the above assumption is valid. The significance of thermal stresses in pores and their relationship to confining pressure becomes apparent when the concept of effective pressure is introduced. Effective pressure is the summation of two opposing pressures. The confining, or lithostatic pressure (P_c) at depth, d, results from the weight of the overlying rocks. The pore-fluid pressure (P_f) at the same depth, d, results from the density of the pore fluid. The difference between P_c and P_f defines the effective pressure, P_e, and

$$P_e = P_c - P_f \tag{15}$$

A recent study on the variation of effective pressure with depth in the crust has been presented by Knapp and Knight (in prep.). The authors show that in many geologic environments the effect of pore-fluid expansion, causing an increase in P_f, cannot be neglected. Increasing P_f will cause the effective pressure to decrease. Because of the low tensile strength of rocks, when effective pressure is reduced to zero the rock will fracture (Knapp and Knight, in prep.). Thus, an increase in porosity is expected at zero effective pressure.

Knapp and Knight (in prep.) have calculated the quantity which defines the rate at which pressure varies with temperature at constant volume for the H_2O system. Values obtained for this coefficient are between 10 bars/^{o}C to 25 bars/^{o}C for all crustal conditions to 30 km depth. The positive coefficient indicates that as temperature is increased the pore-fluid pressure will increase. In an isolated pore at constant confining pressure, as the temperature is increased, the pressure inside the pore will increase until the pore-fluid pressure equals the confining pressure. At this point, the rock will fracture, causing an increase in pore volume (porosity). Further increases in temperature will result in further increases in pore volume. The final configuration of the pores after a breaking event does not imply that all the residual porosity is converted into through-going cracks and fractures. Although the increase in ϕ_F and ϕ_D due to a breaking event is important for fluid flow considerations, the intrinsic resistivity is assumed in this study to vary with the total porosity, and the relative changes in ϕ_F, ϕ_D, and ϕ_R are not considered.

Archie's Law predicts that the intrinsic rock resistivity has a $(\text{porosity})^{-2}$ dependence. The porosity-temperature variation within the upper few kilometers of the crust due to a thermal heat source at depth will be derived following the concept of Knapp and Knight (in prep.). The significance of this porosity increase becomes apparent in geothermal areas, where near-surface temperatures might increase by 200^{o}C. Coupled with the porosity increase with temperature is the pore-fluid resistivity decrease with temperature. Together these effects will result in a

dramatic decrease in intrinsic resistivity in the areas of maximum temperature increase.

The total derivative of volume at constant composition for the rock-pore region in Figure 9 is

$$dV = \left(\frac{\partial V}{\partial T}\right)_P dT + \left(\frac{\partial V}{\partial P}\right)_T dP \tag{16}$$

where $V = V_r + V_f$ and V_r is rock volume while V_f is pore volume. The coefficients of isobaric thermal expansion (α) and isothermal compressibility (β) are defined as

$$\alpha = \frac{1}{V}\left(\frac{\partial V}{\partial T}\right)_P \tag{17a}$$

$$\beta = \frac{-1}{V}\left(\frac{\partial V}{\partial P}\right)_T \tag{17b}$$

Substitution of equations (17a-b) into equation (16) defines the total volume change in terms of α and β:

$$dV = V\,\alpha\,dT - V\,\beta\,dP \tag{18}$$

The total isobaric thermal expansion coefficient (α) may be defined in terms of its components, V_r and V_f:

$$\alpha = \frac{1}{V}\left(\frac{\partial V_r}{\partial T} + \frac{\partial V_f}{\partial T}\right)_P \tag{19}$$

and

$$dV = dV_f + dV_r \tag{20}$$

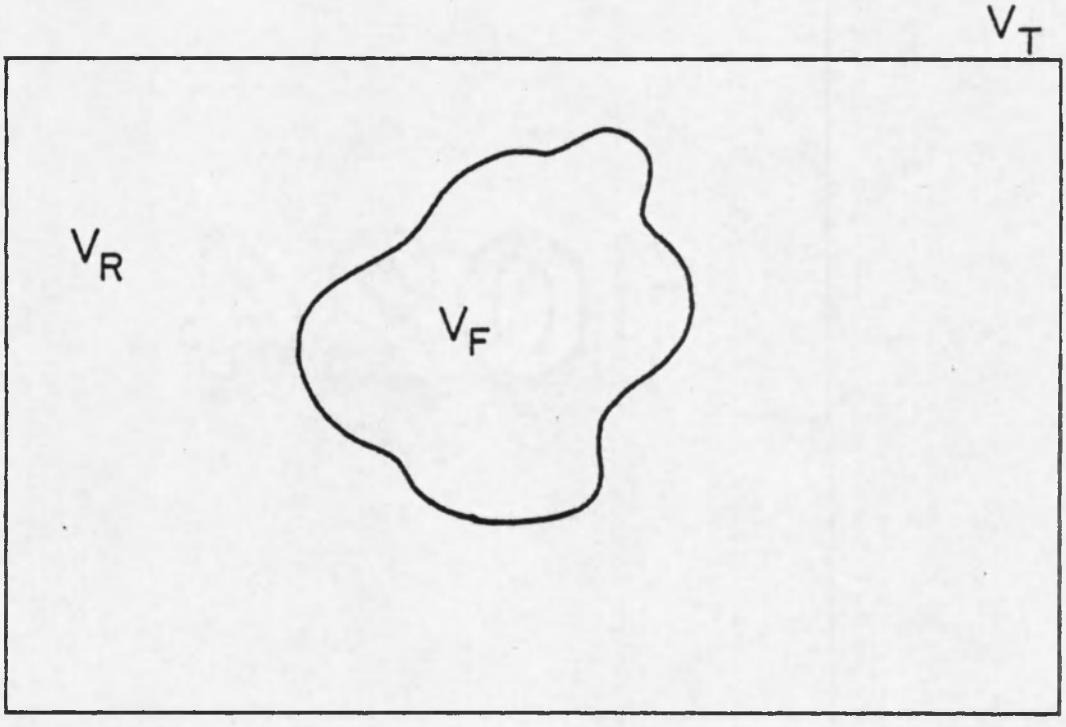

Figure 9. Pore-Rock Region. -- V_R is volume of rock, and V_F is volume of pore.

Comparable expressions to equations (17a,b) may be written for α_f, the thermal expansion of the pore fluid, and α_r, the thermal expansion of the rock. The coefficients, α_f and α_r, can be substituted into equation (19) to yield

$$\alpha = \frac{1}{V}(V_f\alpha_f + V_r\alpha_r) \tag{21}$$

A similar expression to equation (21) can be derived for the total isothermal compressibility, β:

$$\beta = \frac{1}{V}(V_f\beta_f + V_r\beta_r) \tag{22}$$

When equations (22) and (21) are substituted into equation (18), the total volume change becomes

$$dV = (V_f\alpha_f + V_r\alpha_r)dT - (V_f\beta_f + V_r\beta_r)dP \tag{23}$$

However, when the rock initially fractures as a consequence of pore-fluid expansion, an infinitesimal change in pressure will yield further fracturing. Therefore, $dP \tilde{=} 0$ and equation (23) may be simplified to

$$dV = (V_f\alpha_f + V_r\alpha_r)dT \tag{24}$$

Typical values for α_r, for common silicate minerals, over a temperature range of 0-800°C, are on the order of $10^{-6}/^{\circ}C$ (Clark, 1966). The thermal expansion coefficient for pure water, over the same temperature span, is on the order of $10^{-3}/^{\circ}C$. As long as pore volume, V_f, is .01 or greater (total porosities >1%), $V_f\alpha_f >> V_r\alpha_r$ and equation (24) becomes

$$dV = V_f \alpha_f dT \tag{25}$$

The total volume change according to equation (25) occurs as a result of pore volume change, with rock volume remaining essentially constant. Substitution of equation (20), with $dV_r = 0$, into equation (25) yields

$$dV_f = V_f \alpha_f dT \tag{26}$$

Rearranging equation (26) yields an integral equation relating pore volume and temperature

$$\int_{V_f^o}^{V_f} \frac{dV_f}{V_f} = \int_{T_b}^{T} \alpha_f(T)\,dT \tag{27}$$

In equation (27), V_f^o is the initial pore volume and T_b is the temperature at which the rock initially breaks. Integrating equation (17) gives the pore volume as a function of temperature above T_{Bk}

$$V_f = V_f^o \exp\left[\int_{T_b}^{T} \alpha_f(T)\,dT\right] \tag{28}$$

A more general expression for equation (28), to allow for temperatures below T_b, can be written by using a unit step function. The unit step function is defined as

$$h(T - T_b) = \begin{cases} 0 & T < T_b \\ 1 & T \geq T_b \end{cases} \tag{29}$$

When equation (29) is introduced into the integral of equation (28), the pore volume-temperature function for all T is

$$V_f = V_f^o \exp\left[\int_{T_b}^{T} h(T - T_b)\alpha_f(T)dT\right] \tag{30}$$

The initial porosity, ϕ_T^o, is defined as

$$\phi_T^o = \frac{V_f^o}{V_r + V_f^o} = \frac{V_f^o}{V^o} \tag{31}$$

and

$$V^o = V_r + V_f^o \tag{32}$$

Solving equations (31) and (32) for V_f^o and V_r results in the following expressions

$$V_r = (1 - \phi_T^o)V^o \tag{33a}$$

$$V_f = \phi_T^o V^o \tag{33b}$$

Substitution of equation (30) into equation (31) defines the porosity temperature function

$$\phi_T^o = \frac{V_f^o \exp\left[\int_{T_b}^{T} h(T - T_b)\alpha_f(T)dT\right]}{V_r + V_f^o \exp\left[\int_{T_b}^{T} h(T - T_b)\alpha_f(T)dT\right]} \tag{34}$$

Initially, the temperature is below T_b, and equation (34) reduces to equation (31). As T becomes greater than T_b, the porosity, ϕ_T^o, is no longer constant and equation (34) becomes

$$\phi_T = \frac{V_f \exp\left[\int_{T_b}^{T} h(T - T_b)\alpha_f(T)dT\right]}{V_r + V_f \exp\left[\int_{T_b}^{T} h(T - T_b)\alpha_f(T)dT\right]} \tag{35}$$

Letting $F(T) = \exp\left[\int_{T_b}^{T} h(T - T_b)\alpha_f(T)dT\right]$, and substituting equations (33a,b) into equation (35), the porosity-temperature function in terms of the initial porosity becomes

$$\phi = \frac{\phi_T^o F(T)}{(1 - \phi_T^o) + \phi_T^o F(T)} \tag{36}$$

For the purposes of this study, equation (36) defines increaeses in the effective electrical porosity. That is, all porosity increases due to thermal effects are assumed to contribute to increased electrical current flow in rocks. Therefore, equation (36) may now be directly substituted into Archie's Law to account for the variability of porosity with space and time in the host rocks around a cooling pluton.

Numerical Approximation of Porosity-Temperature Function

The integral in F(T) may be approximated by using Simpson's Rule:

$$\int_{T_b}^{T} h(T - T_b)\alpha_f(T)dT \tilde{=} h(T - T_b)\sum_{T_b}^{T} \frac{\alpha_f(T) + \alpha_f(T + \Delta T)}{2}\Delta T \qquad (37)$$

Equation (36) may be discretized for numerical computation with the inclusion of equation (37)

$$\phi_{i+1} = \frac{\phi_i \exp\left[\frac{T_{i+1} - T_i}{2}(\alpha_f(T_i) + \alpha_f(T_{i+1}))\right]}{1 - \phi_i + \phi_i \exp\left[\frac{T_{i+1} - T_i}{2}(\alpha_f(T_i) + \alpha_f(T_{i+1})\right]} \qquad (38)$$

where ϕ_{i+1} is the new porosity at T_{i+1}, and ϕ_i is the old porosity at T_i. The breaking temperature, T_b, may be defined as

$$T_b = T_A + \Delta T \qquad (39)$$

where T_A is the ambient temperature and ΔT is the temperature increment added to T_A in order to reduce effective pressure to zero. ΔT will depend directly on the geothermal gradient (Knapp and Knight, in prep.). The maximum value for ΔT (ΔT_{max}) along a geothermal gradient of $20^{o}C/km$ is $20^{o}C$ (R. Knapp, personal communication, 1976). For shallower geothermal gradients, $\Delta T_{max} > 20^{o}C$ and for steeper geothermal gradients $\Delta T_{max} < 20^{o}C$. In the present study, a geothermal gradient of $20^{o}C/km$ is chosen, and $\Delta T_{max} = 20^{o}C$ will be used.

Figure 10 shows the porosity-temperature function defined by equation (38) at 1 and 2 km below the earth's surface. The nature of these curves is as follows: Given an initial breaking temperature, T_b,

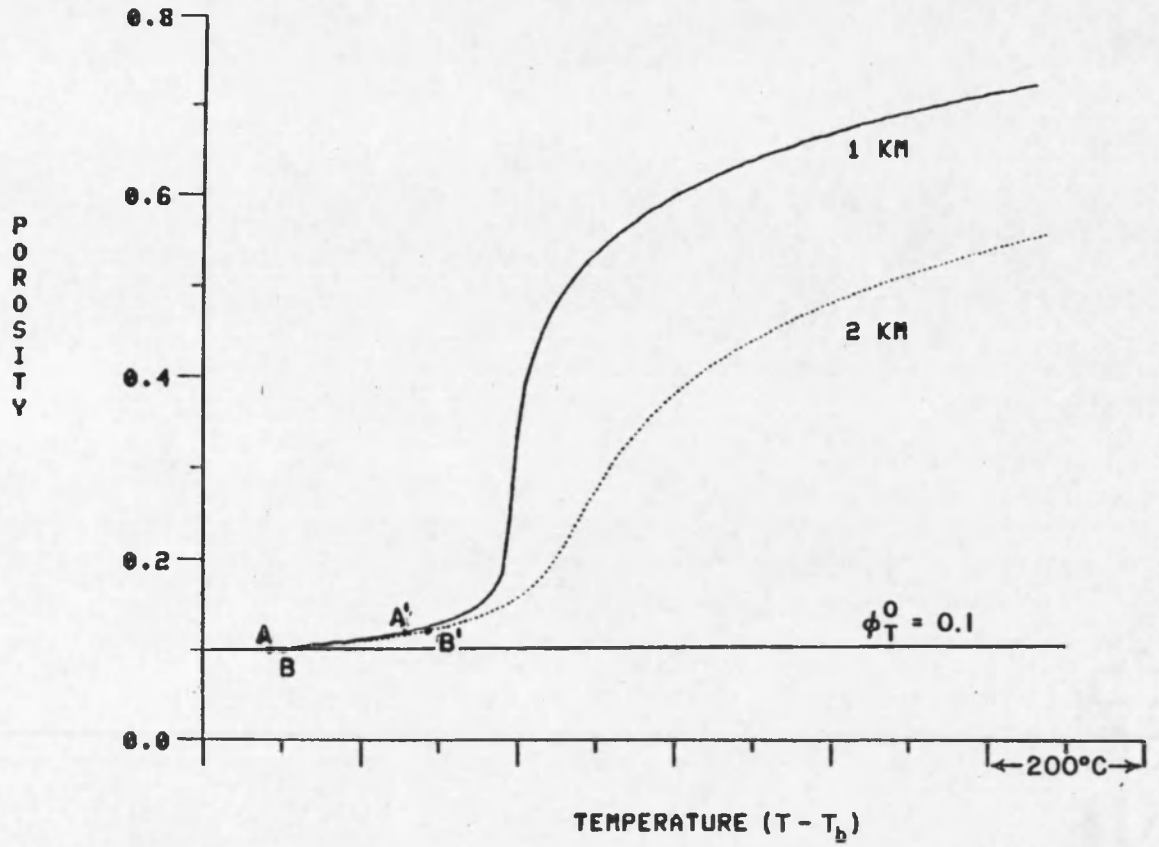

Figure 10. Porosity as a Function of Temperature Defined by Equation (38). -- The 1 km (2 km) curve represents the porosity increase starting from an initial temperature defined by A(B). A-A' and B-B' represent porosity increases due to a $T-T_b=200^oC$, where $T-T_b$ are the integration limits in equation (38).

at point A, a temperature increase of $T-T_b = 200^oC$ will produce a porosity increase to point A'. Increasing T_b to point B on the 2 km depth curve, the same temperature increase of $T-T_b = 200^oC$ will result in a final porosity of B'. For initial breaking temperatures, $T_b < 120^oC$, the porosity increase is very slight for small changes in temperatures ($T-T_b < 100^oC$). In this study, Archie's Law is assumed to be an adequate first order approximation for rock resistivity; therefore, the important parameter in predicting resistivity is $1/\phi_T^2$, so that a very small increase in porosity will result in a significant decrease in ρ_R. Figure 11 shows the $1/\phi_T^2$ dependence for a $T_b = 60^oC$ (1 km depth curve in Figure 10). For the same $T-T_b = 200^oC$ in Figure 10, $1/\phi_T^2$ is decreased by 30%. Therefore, the effect of the porosity increase is enough to reduce the intrinsic resistivity by 30%.

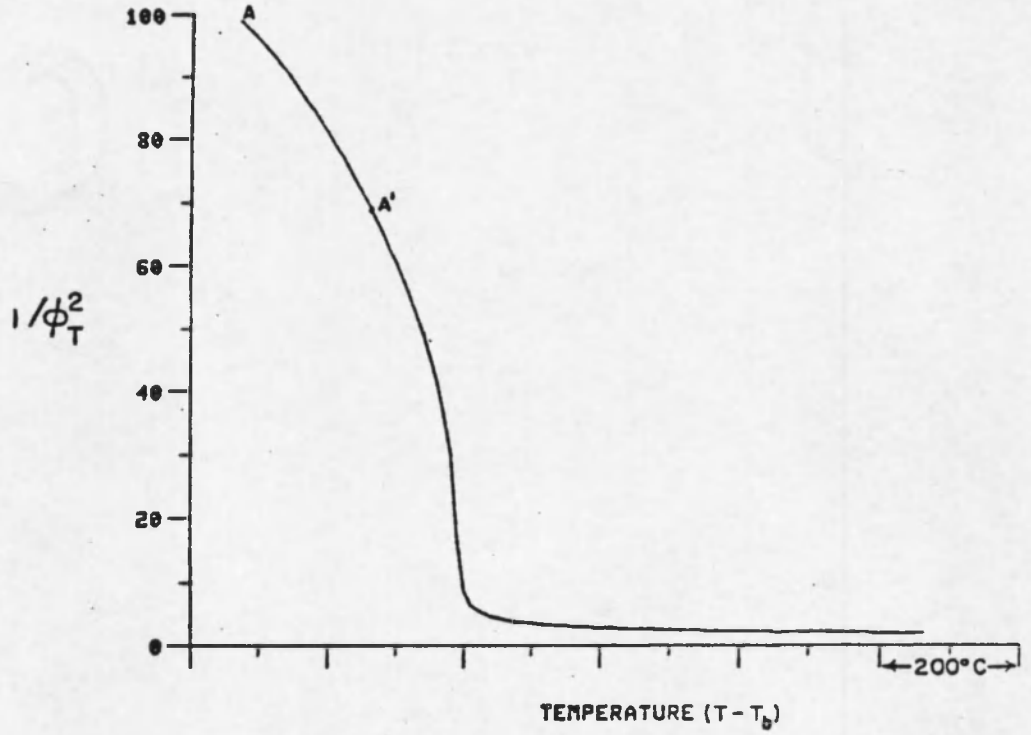

Figure 11. $^1/\phi_T^2$ as a Function of Temperature. -- A-A' represents decrease in $^1/\phi_T^2$ due to a $T-T_b=200^oC$.

COMPUTER MODELS

Intrinsic rock resistivity, calculated by Archie's Law, varies directly with pore-fluid resistivity and inversely with porosity. The behavior of fluid resistivity over the range of temperatures and pressures prevailing in the upper 10 km of the crust has been discussed previously. The porosity increase in response to a thermal perturbation was derived and is defined by equation (38). However, the porosity-temperature function may only be applied when there is an increase in initial temperature. For an instant in geologic time, temperatures at a particular depth along geothermal gradients do not vary and equation (38) would be of little use. In a prior study, Brace (1971) modeled crustal resistivity to 40 km, using a combination of water resistivity data, geothermal gradient data, and porosity data. However, Brace's models did not include the transient aspect of crustal resistivity due to the transport of thermal energy away from a heat source. This heat source might be a pluton emplaced at shallow crustal depths, as might be the case in active geothermal areas. The heat source might also be the result of a regional heat flux from the mantle into the crust. Fluid resistivity and the porosity increase due to increasing temperature are primarily functions of temperature. Therefore, intrinsic rock resistivity will be controlled by the crustal distribution of temperance. A necessary first step in the analysis of the time dependence of resistivity within the crust is the modeling of the spacial and temporal distribution of temperature resulting from crustal heat sources.

Using Archie's Law, intrinsic host-rock resistivity has been numerically modeled for two, two-dimensional crustal environments. Pore-fluid resistivities as a function of temperature and pressure, and composition and variations in electrical porosity as a function of temperature have been computed for two crustal environments characterized by pluton emplacement within the upper 10 km of the surface. In the first model the crustal system cools by pure conductive heat transfer, whereas the second model cools dominantly by convective heat transfer. The conductive and convective dominated systems have been numerically modeled according to a set of partial differential equations described in Norton and Knight (in press). The primary purpose of this chapter is to describe the crustal resistivity models. The governing partial differential equations and their numerical approximations will also be discussed.

Governing Equations

Implicit in the intrinsic resistivity models is the two-dimensional numerical analysis of a cooling pluton within the upper crust. The most extensive attempt at numerical modeling of cooling plutons is described in Norton and Knight (in press). These models treat the two-dimensional cross section of the crust as a fluid-saturated permeable media. The models afford for variation in permeability and porosity, heat sources, fluid and rock properties, as well as the time dependence of a cooling pluton. The thermal anomaly produced by pluton emplacement is dispersed by means of conductive and convective heat transfer processes. A complete description of the governing equations,

their physical significance, and numerical approximations is given in Norton and Knight (in press).

The partial differential equations which adequately describe the heat transfer and fluid flow processes occurring within the upper crust are

$$(C_m\rho_m + a)\frac{\partial T}{\partial t} + \bar{q}\nabla C_f T = \nabla\cdot(K_m \nabla T) \tag{40}$$

$$\nabla\cdot\bar{q} = 0 \tag{41}$$

$$\nabla^2\Psi + \frac{1}{K}\left[\frac{\partial\Psi}{\partial y}\frac{\partial K}{\partial y} + \frac{\partial\Psi}{\partial z}\frac{\partial K}{\partial z}\right] = \frac{\partial\rho}{\partial y} \tag{42}$$

Table 3 is a list of the above variables and their definitions. Equations 40 to 42 form a set of three equations with three unknowns. The unknowns are the dependent variables: temperature (T), fluid flux (q), and stream function (Ψ). The numberical approximations to these equations, using finite differences, are solved by the alternating-direction implicit method (Norton and Knight, in press).

The fluid properties for these models were approximated by the H_2O system. The fluid transport properties, except fluid viscosity, were computed from equations of state given by Keenan, Keyes, Hill, and Moore (1969) and Helgeson and Kirkham (1974). Fluid viscosity data were computed from equations modified from Burges, Latto, and Ray (1966). Fluid resistivity data were obtained from tables modified from Quist and Marshall (1968), Gunning and Gordon (1942), and Chambers (1958). Rock properties (e.g., heat capacity, density, heat of crystallization, radioactive decay constants, hydrolysis reactions, etc.) were estimated from

Table 3. Definition of Variables and Constants Appearing in Governing Equations for Heat Transfer Process Associated with Thermal Perturbations in the Crust.

VARIABLE	DEFINITION	UNITS
C_m	heat capacity at constant pressure of the media	cal g^{-1} $^oC^{-1}$
ρ_m	density of media	gr $\cdot$ cm^{-3}
a	volumetric heat source	cal cm^{-3} $^oC^{-1}$
C_f	isobaric heat capacity of fluid	cal g^{-1} $^oC^{-1}$
K_m	thermal conductivity of media	cal cm^{-1} sec^{-1} $^oC^{-1}$
$\overline{q}$	fluid flux vector	g cm^{-2} sec^{-1}
T	temperature	^oC
Ψ	stream function	g cm^{-1} sec^{-1}
ρ	fluid density	gr cm^{-3}
$K(=\frac{\upsilon}{\kappa})$	viscosity (υ) permeability (κ)	cm^2/sec cm^2
g	gravitational force vector	cm sec^{-2}
$\overline{\nabla}$	$\frac{\partial}{\partial x}\hat{i} + \frac{\partial}{\partial y}\hat{j} + \frac{\partial}{\partial z}\hat{k}$	

table values for igneous and sedimentary rocks (Clark, 1966). Rock permeability was estimated from analytical equations and experimental data (Norton and Knight, in press). Rock porosity data was estimated from equation (38), which relates initial porosity to temperature increase and experimental data (Norton and Knapp, in prep.). These models examine ranges in parameters since intrinsic rock permeability and porosity values are not available. Therefore, the results probably do not have exact natural analogues.

Coupled with the numerical solution of the governing partial differential equations, an interactive graphics system was developed in order to present the model results in a coherent fashion. The interactive graphics system allows the user to time step through a given model, stopping at specified times to analyze the steady-state solutions of equations 40-42. Through the use of this graphics system, two heuristic models, P1 and P3, taken from Norton and Knight (in press), have been used to numerically model host-rock resistivity as a function of space and time. Model P1 is characterized by low permeability (10^{-17} cm^2) which inhibits convective heat transfer. In model P3 the permeability of the host rocks was increased to 10^{-11} cm^2. This results in a convective-dominated heat transfer process within the host rocks. The P3 pluton is impermeable (10^{-14} cm^2) and therefore cools conductively. Both models have initial porosities of .01. However, the porosity is allowed to vary as a function of temperature, according to equation (38). The pore fluid is assumed to be saline water with a concentration of .01 molal, and gradients in fluid composition are not explicitly accounted for in the computations.

Conductive Model

Model P1 is characterized by a constant permeability of 10^{-17} cm^2. This low permeability inhibits fluid flow within the host rocks and thereby results in a pure conductive cooling history. The cross-section of the P1 pluton is rectangular in shape with a width of 4 km and a height of 4.5 km. The P1 pluton is emplaced at a depth of 4.5 km and the emplacement temperature is 870°C. The initial thermal gradient in the host rocks is 20°C/km. The boundary conditions which must be specified in order to solve the governing equations involve thermal and fluid flux conditions. Thermal boundary conditions are required for the solution of equation (40), while fluid flux conditions are necessary for solution of equation (42). The initial and boundary conditions for model P1 are shown in Figure 12. The conductive temperature boundary condition requires that temperature is constant with time along a boundary. This condition is applied to the top boundary of the model (earth's surface). The insulating boundary condition requires that heat flux through a boundary be zero. This boundary condition is maintained along the left, right, and bottom boundaries of the P1 model. The fluid flux boundary condition of no flow prohibits fluid flow across a boundary. This boundary condition is applied to all four boundaries. Also shown in Figure 12 are locations of vertical sections (dash lines) and locations of points where the time variation of resistivity and porosity will be calculated (circles).

The thermal history of the P1 pluton and its surrounding host rocks is shown in Figure 13. The temperature distribution in model P1 is characterized by broad isotherms which are convex upward. The

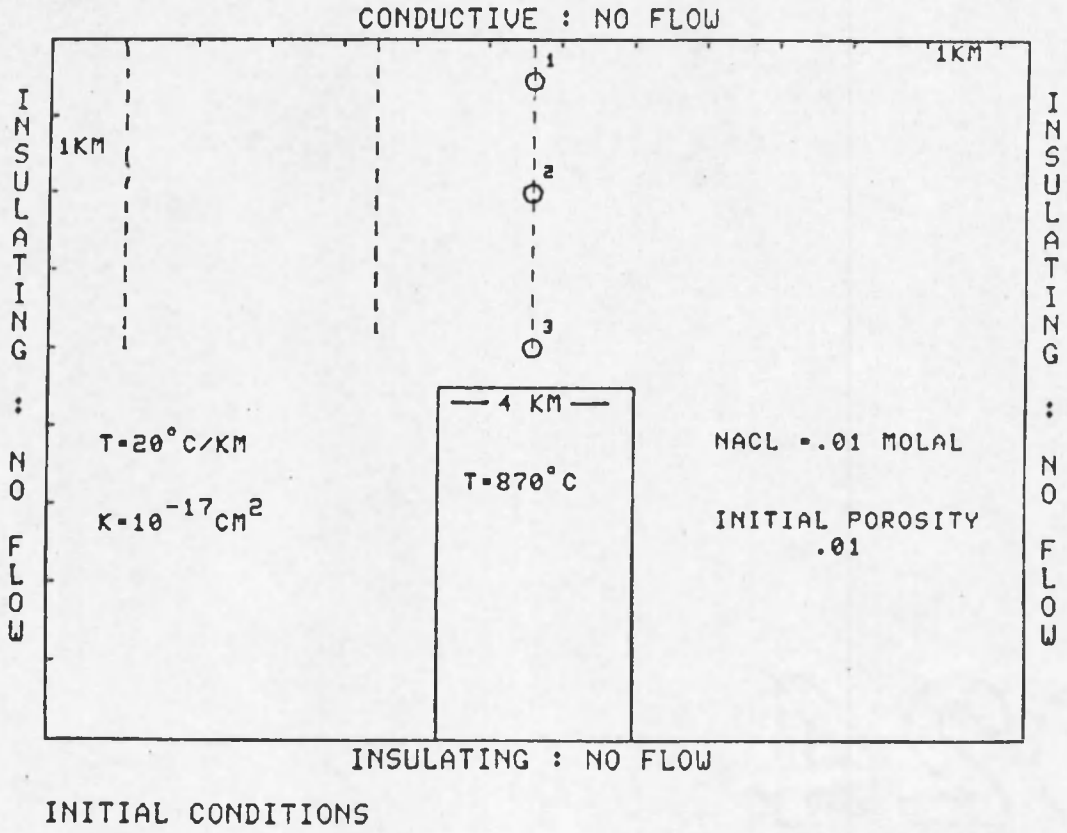

INITIAL CONDITIONS

Figure 12. Two-dimensional Cross-section of Model P1 Describing Initial and Boundary Conditions. -- Pluton is shown as rectangular body in center of figure. Dash lines denote locations where vertical profiles will be calculated and circles represent fixed points where the time variations in porosity and resistivity will be calculated. Also shown are K, permeability, T = 20°C/km, initial thermal gradient and T = 870°C, the initial pluton temperature. The origin corresponds to upper left hand corner. The top boundary is taken to be the earth's surface. The model is symmetric about the pluton's midpoint in the horizontal direction.

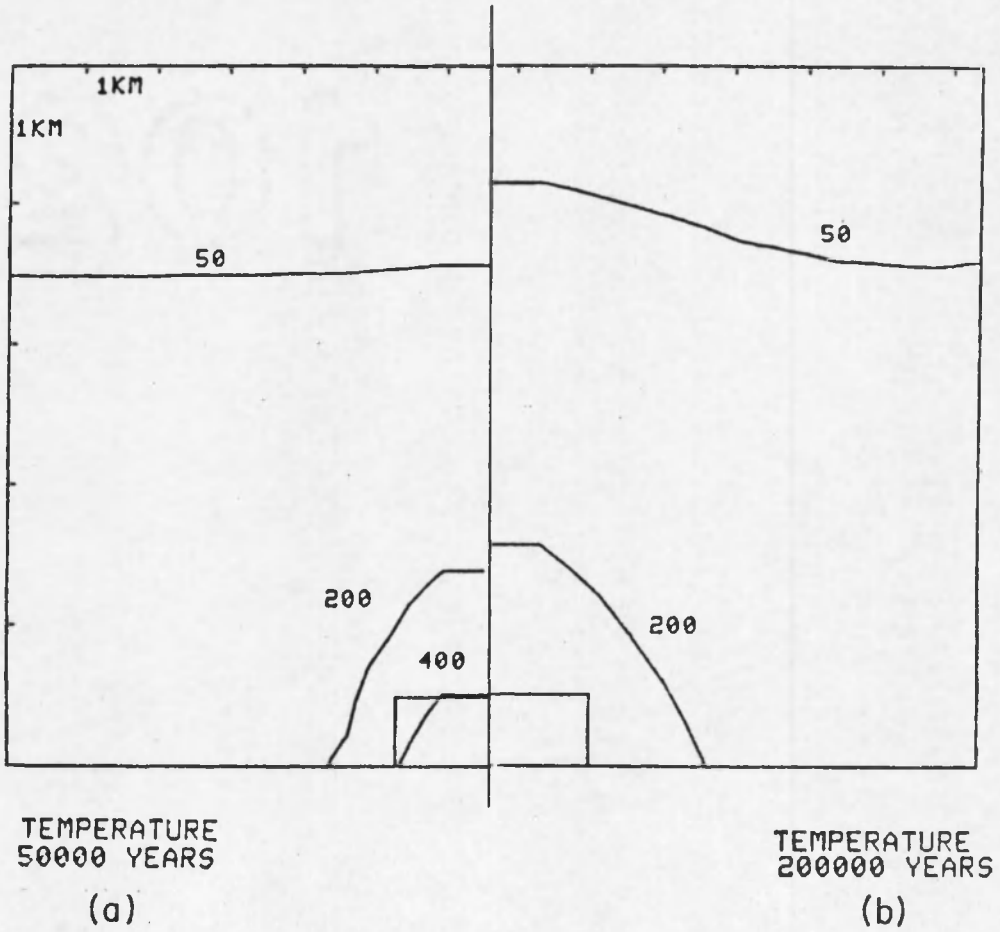

Figure 13. Steady-state Temperature (^{o}C) Distribution at (a) 50,000 Years and (b) 200,000 Years in Model P1.

isotherms also tend to be subparallel to the top and sides of the pluton. During the initial 50,000 years the temperature maximum migrates upward from the top of the pluton at a rate of 2 cm/yr. The rate of upward migration of the temperature maxima decreases to .5 cm/yr by 200,000 years (Norton and Knight, in press). The spacial and temporal distribution of isotherms will directly influence the pore-fluid resistivity and the porosity of the host rocks. Before emplacement of the P1 pluton at 4.5 km depth, the initial temperature at this depth was 110°C (defined by the 20°C/km geothermal gradient). At 200,000 years after pluton emplacement, the 200°C isotherm is at approximately 3.5 km depth (Figure 13b). This means that points between the top of the pluton and the 200°C isotherm are now above 200°C and temperatures within this zone have increased by at least 90°C. The significance of this 200°C isotherm and the zone between this isotherm and the top of the pluton becomes apparent when changes in pore-fluid resistivity and porosity are analyzed. The pore-fluid resistivity will reach a minimum at temperatures between 200°C-300°C (Figure 4). The porosity increase defined by equation (38) will be approximately 10% for temperature increases of 100°-200°C. Therefore, the zone between the 200°C isotherm and the top of the pluton in the P1 system will be characterized by maximum porosity increase and the maximum decrease in pore-fluid resistivity. Thus, the maximum porosity increase will occur where the temperature increase is a maximum and, if this temperature maxima is between 200°-300°C, the pore-fluid resistivity will also be a minimum. Before presenting the results of the host-rock resistivity distribution in the P1 model, the

spatial and temporal distribution of porosity in this model will be discussed.

The porosity variation with depth for model P1 is shown in Figures 14 and 15. The vertical lines along which these depth profiles were calculated are shown in Figure 12. The maximum increase in porosity occurs at 50,000 years (Figure 14). This porosity increase is approximately 20% and is located directly over the pluton. At 200,000 years (Figure 15), the maximum increase in porosity is again directly over the pluton. However, due to thermal decay of the P1 system, the porosity maxima has decreased by 10% from its value at 50,000 years. Even at 200,000 years after pluton emplacement, there is no porosity variation with depth until depths of 1.5-2 km. This observation is more evident when the time variation of porosity is calculated at fixed points 4, 2.5, and .5 km above the top of the pluton. These points are shown by circles in Figure 12, and the resulting porosity variation is illustrated in Figure 16. The only major variation in porosity occurs during the initial 40,000 years, where a 20% porosity increase occurs at .5 km above the pluton (curve 3). However, for the time duration of the model, no appreciable change in porosity occurs at depths <2 km (curves 1 and 2). As illustrated in Figure 13, the upper 2 km in the P1 system is characterized by very little variation from the normal geothermal gradient. Thus, there is no significant change in porosity within this zone.

The distribution of isotherms in space and time, which directly affects the pore-fluid resistivity and the porosity, will determine the host-rock resistivity distribution. Figures 17 and 18 contrast the

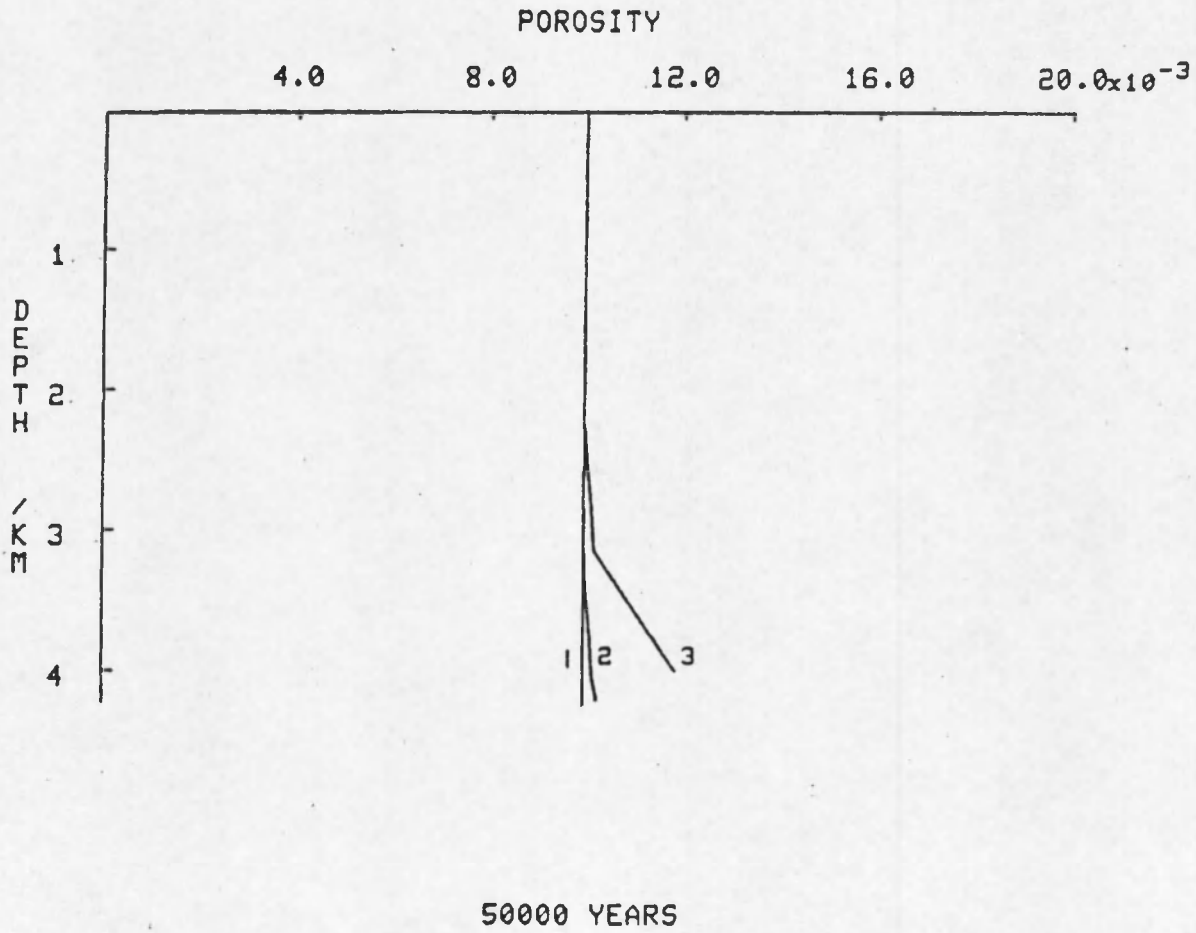

Figure 14. Vertical Porosity Gradients in Model P1 at 50,000 Years. -- Vertical profiles are located 4.5 km (1), and 1 km (2) from side contact of pluton and through center (3) of pluton.

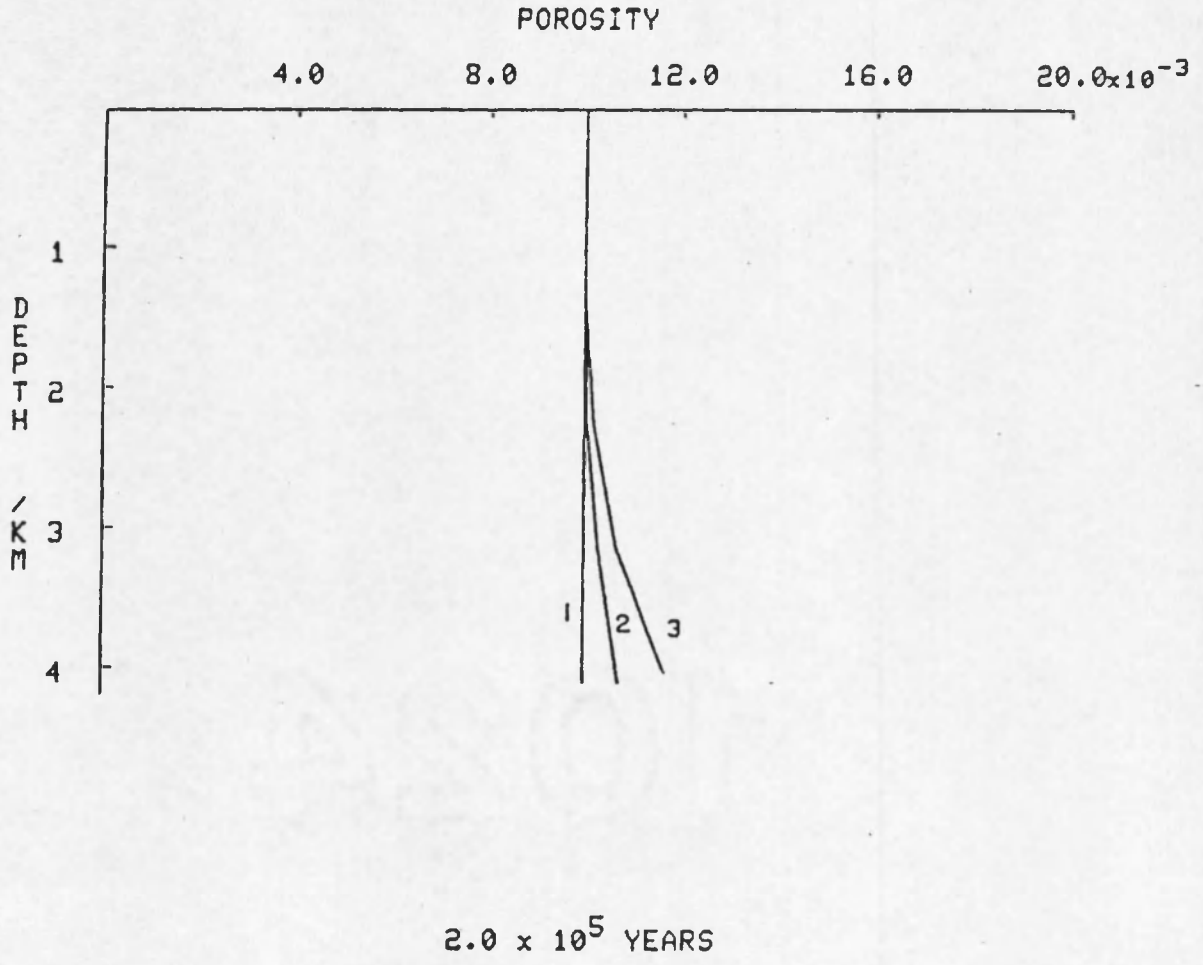

Figure 15. Vertical Porosity Gradients in Model P1 at 200,000 Years. -- Locations of vertical profiles are the same as in Figure 14.

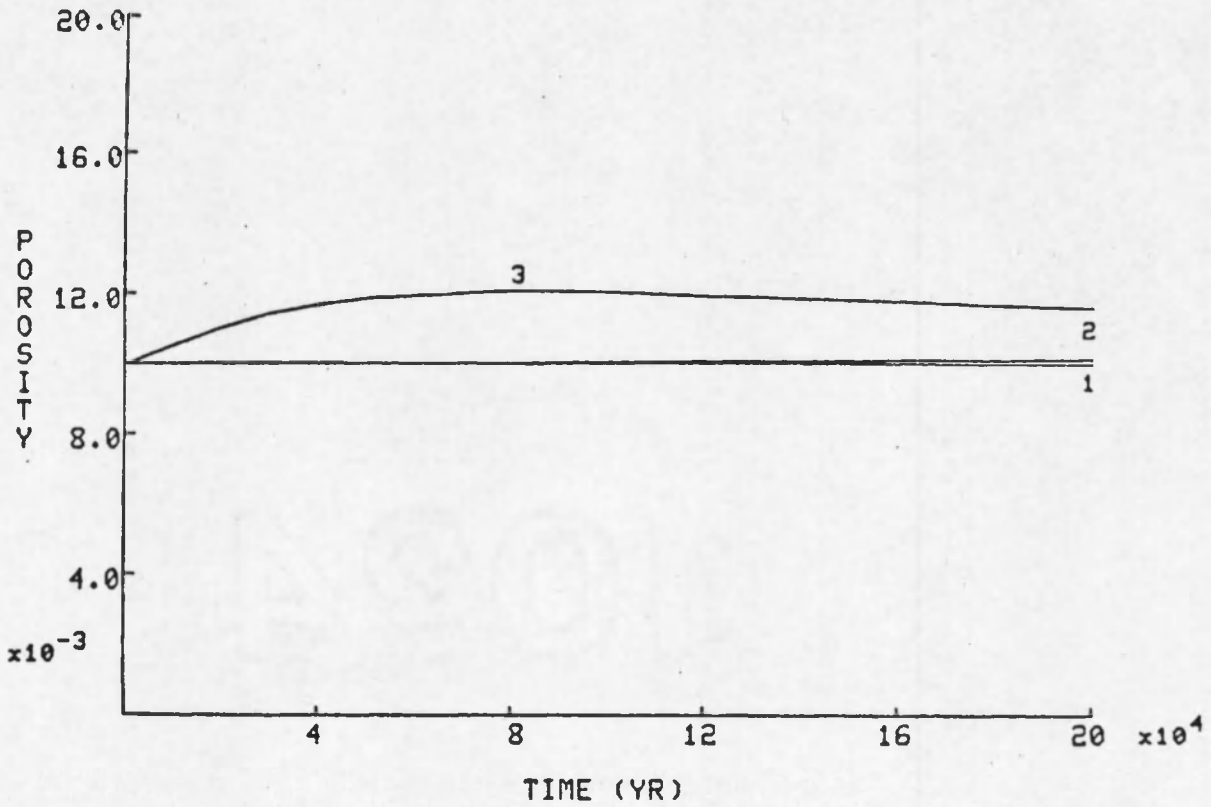

Figure 16. Porosity as a Function of Time in Model P1 at Fixed Points 4 km (1), 2.5 km (2), and .5 km (3) Directly above Top of Pluton.

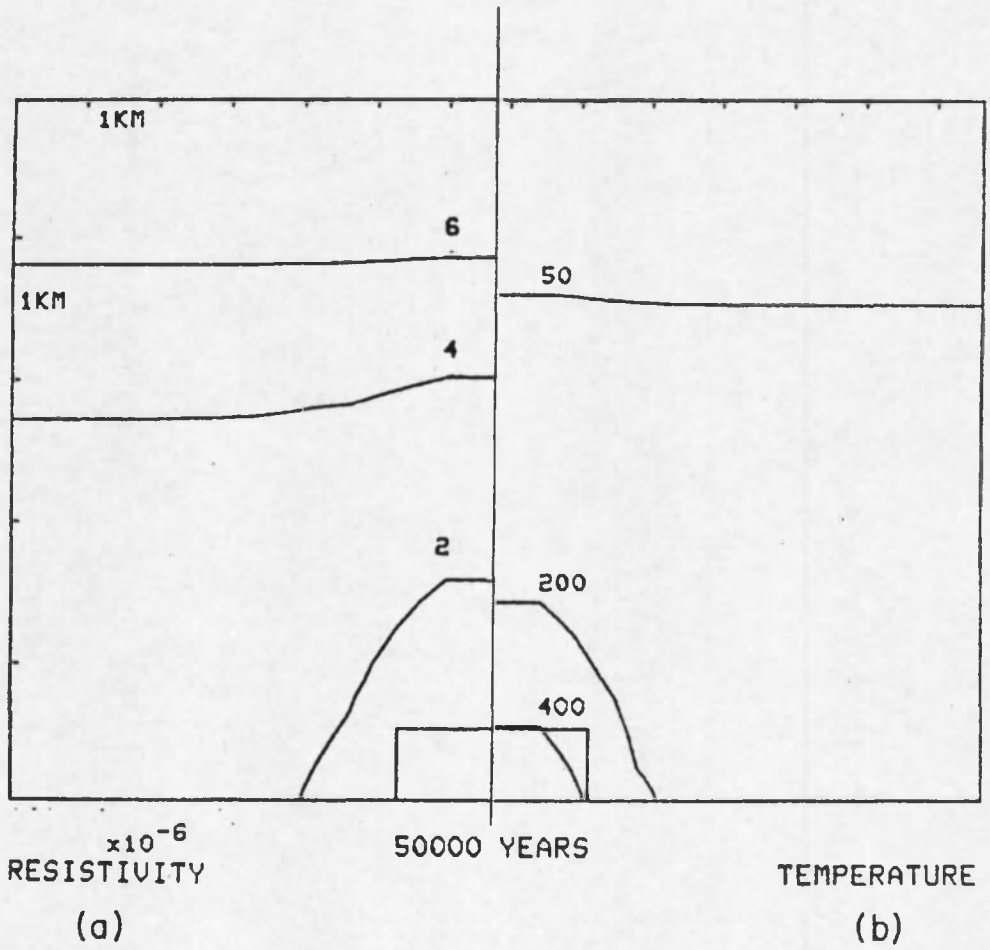

Figure 17. Steady-state (a) Resistivity Distribution (ohm-cm) and (b) Temperature (^{o}C) Distribution in Host Rocks of Model P1 at 50,000 Years.

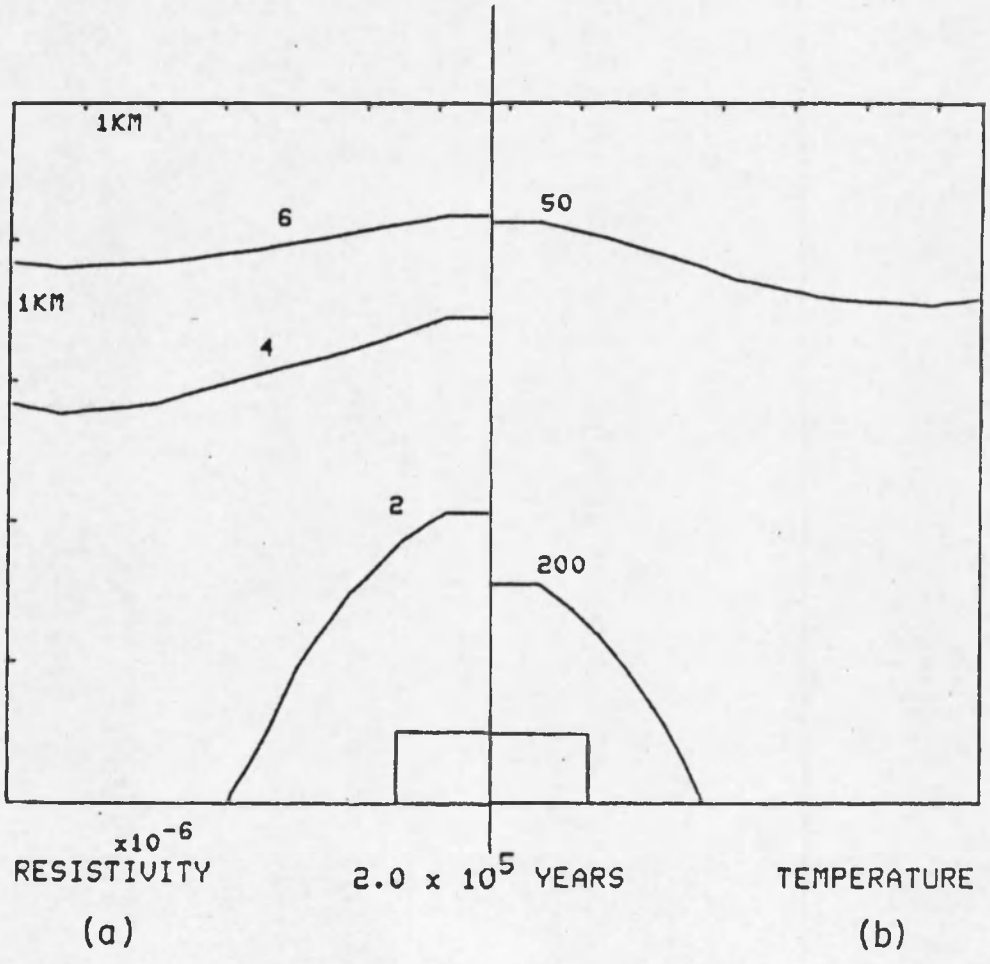

Figure 18. Steady-state (a) Resistivity Distribution (ohm-cm) and (b) Temperature (^{o}C) Distribution in Host Rocks of Model P1 at 200,000 Years.

resistivity isopleths and isotherms at 50,000 and 200,000 years, respectively. The resistivity isopleths parallel the isotherms, being broad, convex upward, and subparallel to the sides and top of the pluton. Figure 19 shows the displacement in the resistivity isopleths between 50,000 and 200,000 years. The rate of upward migration of the resistivity isopleths is a maximum directly over the pluton. The calculated maximum rate of .6 cm/yr decreases to .3 cm/yr at 3 km above the pluton. This rate of upward migration of decreasing resistivity is coincident with the upward migration of the temperature maxima. The decrease in displacement of the resistivity isopleths with distance above the pluton is also coincident with slow upward transport of thermal energy away from the pluton (Norton and Knight, in press).

Resistivity was calculated as a function of depth along lines 1, 2, and 3 of Figure 12, and the resulting resistivity profiles are shown in Figures 20 and 21. Figure 20 shows the variation of resistivity with depth in the host rocks at 50,000 years. The resistivity gradients (curves 2 and 3) are coincident with the background resistivity gradient[1] (curve 1) until a depth of 1.5 km. At 4 km depth directly over the pluton, calculated resistivity values are approximately an order of magnitude less than values calculated from the background resistivity gradient. The resistivity gradients at 200,000 years (Figure 21) are almost identical to the gradients at 50,000 years. However, at 200,000 years the gradients are coincident until a depth of .5 km, as compared to 1.5 km

---

1. Background resistivity gradient due to normal geothermal gradient.

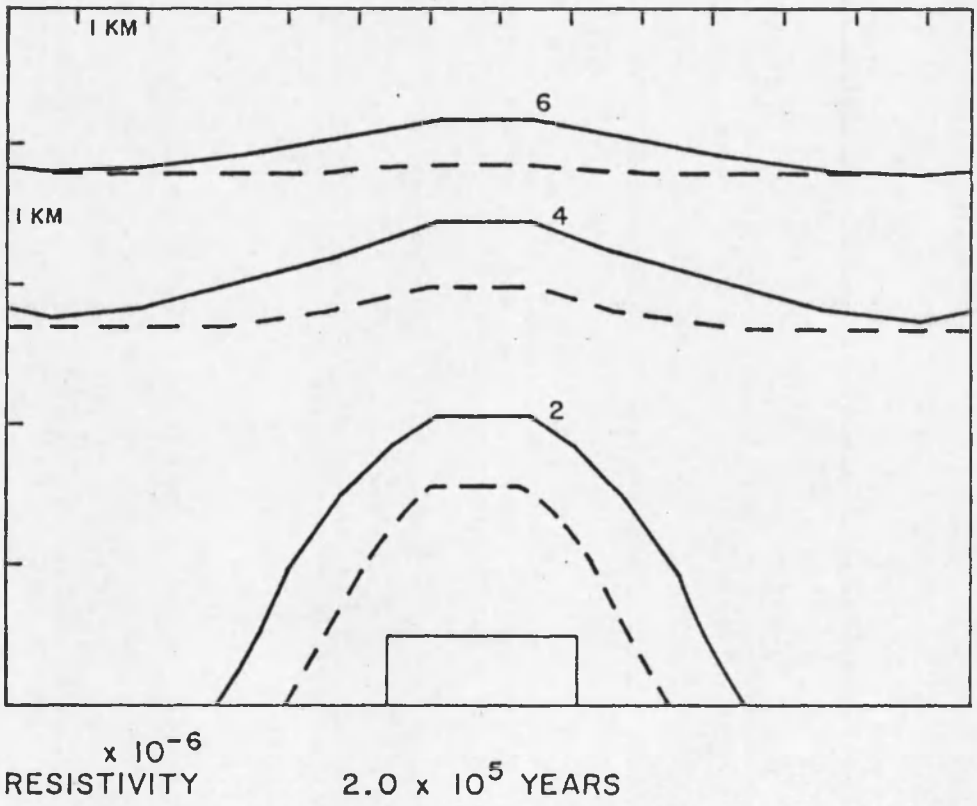

Figure 19. Displacement of Resistivity Isopleths between 50,000 Years (Dash Lines) and 200,000 Years (Solid Lines).

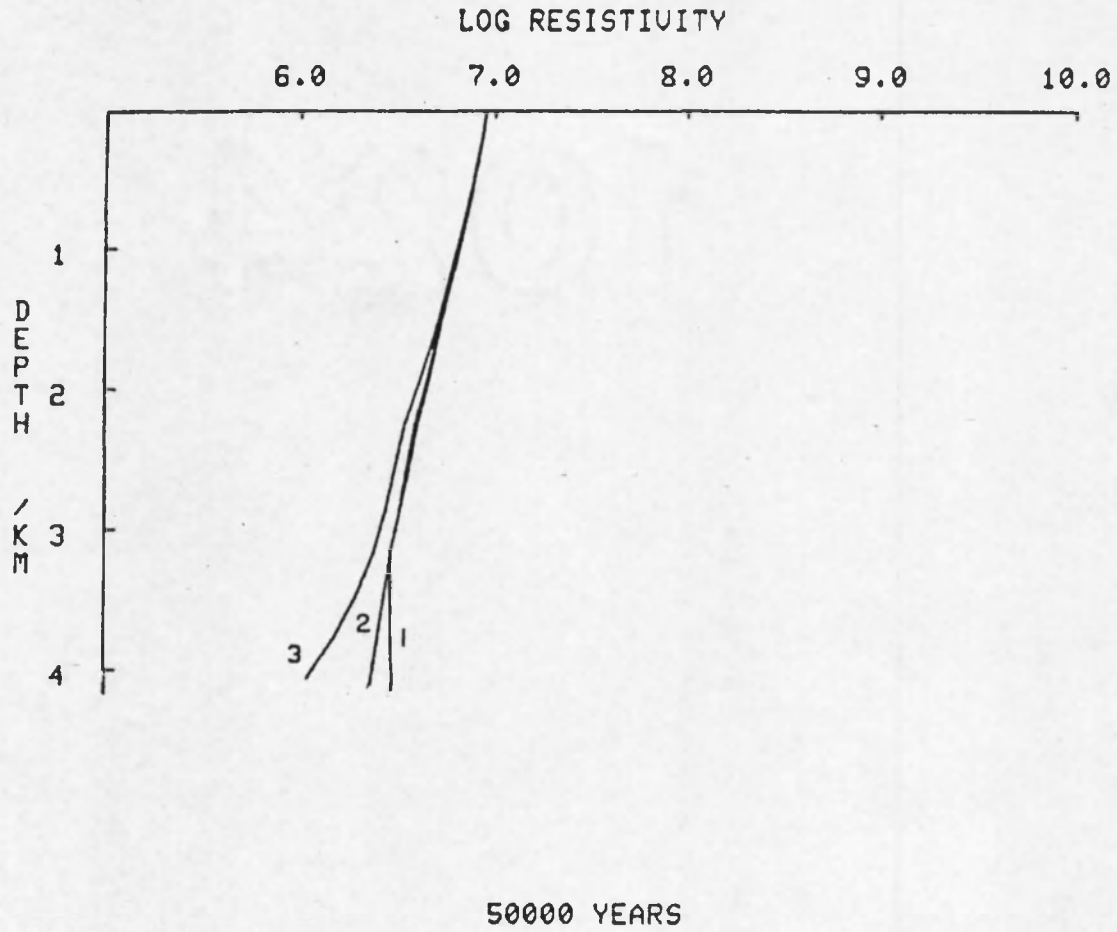

Figure 20. Resistivity (ohm-cm) as a Function of Depth in Model P1 at 50,000 Years. -- Locations of vertical profiles are the same as in Figure 14.

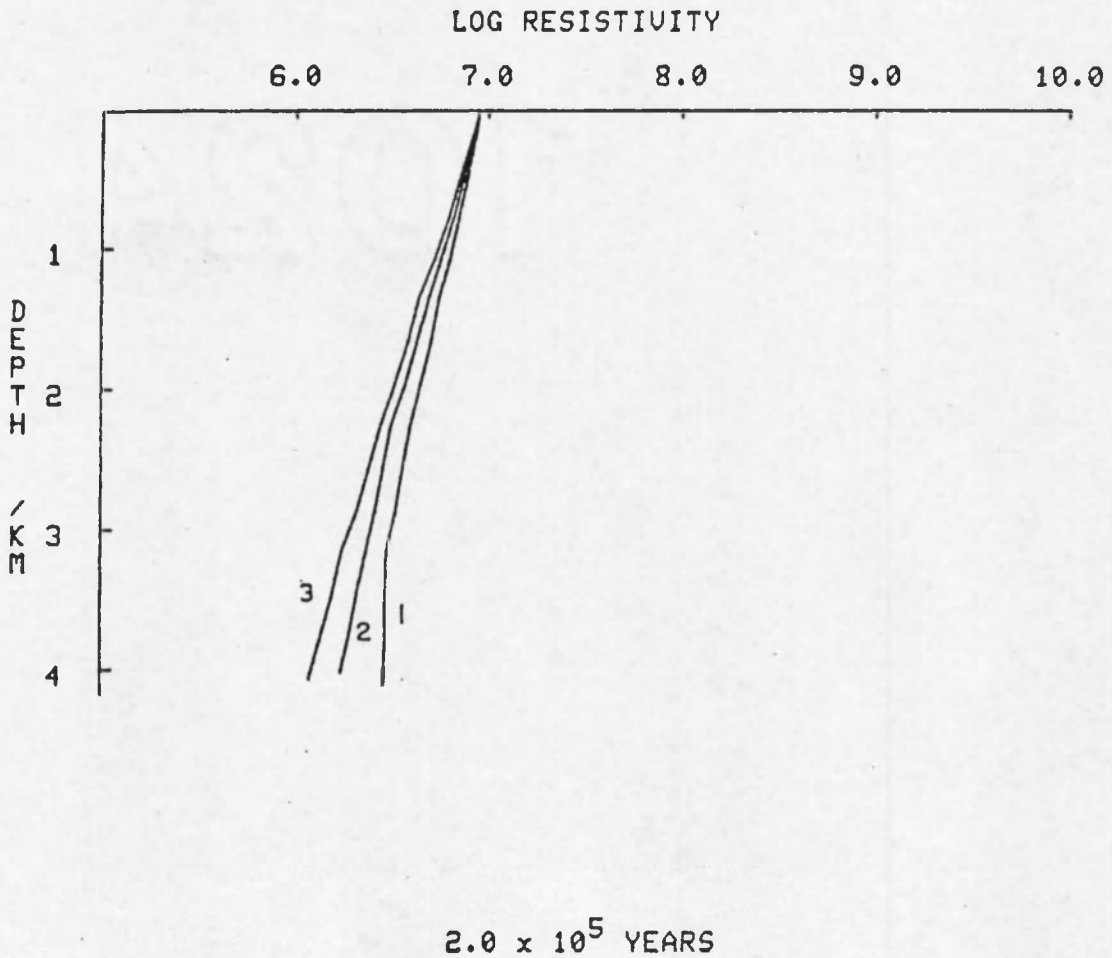

Figure 21. Resistivity (ohm-cm) as a Function of Depth in Model P1 at 200,000 Years. -- Locations of vertical profiles are the same as in Figure 14.

at 50,000 years. At both times resistivity slowly decreases with depth. The resistivity minima occurs directly over the pluton at a depth of 4 km. This resistivity minima is coincident with the porosity maxima (Figures 14 and 15) and the pore-fluid resistivity minima associated with the 200°C isotherm. The maximum host-rock resistivity decrease is by a factor of 10, as compared with surface values. The maximum range in host-rock resistivity is from 10^6-10^7 ohm-cm.

The time variation in resistivity is shown in Figure 22 for fixed points 4, 2.5, and .5 km above the pluton. The only noticeable variation in resistivity occurs directly over the pluton (curve 3), where a decrease by a factor of 5 occurs within the initial 40,000 years. This resistivity decrease correlates with the rapid increase in porosity directly over the pluton (Figure 16), as well as with the temperature maxima over the pluton (Norton and Knight, in press). It is also apparent from Figure 22 that very little variation in host-rock resistivity occurs at depths <2 km by 200,000 years, when emplacement of a pluton at depths >4.5 km is into impermeable host rocks.

Calculations of temperature, porosity, fluid resistivity, and host-rock resistivity for the P1 system indicate that the host-rock resistivity distribution is controlled by the distribution of isotherms. Maximum decreases in host-rock resistivities occur between the 200°C isotherm and the top of the pluton. This is the direct result of the porosity maxima and the pore-fluid resistivity minima within this zone. Also, the negligible variation of host-rock resistivity at depths <2 km is coincident with the negligible temperature increase in this

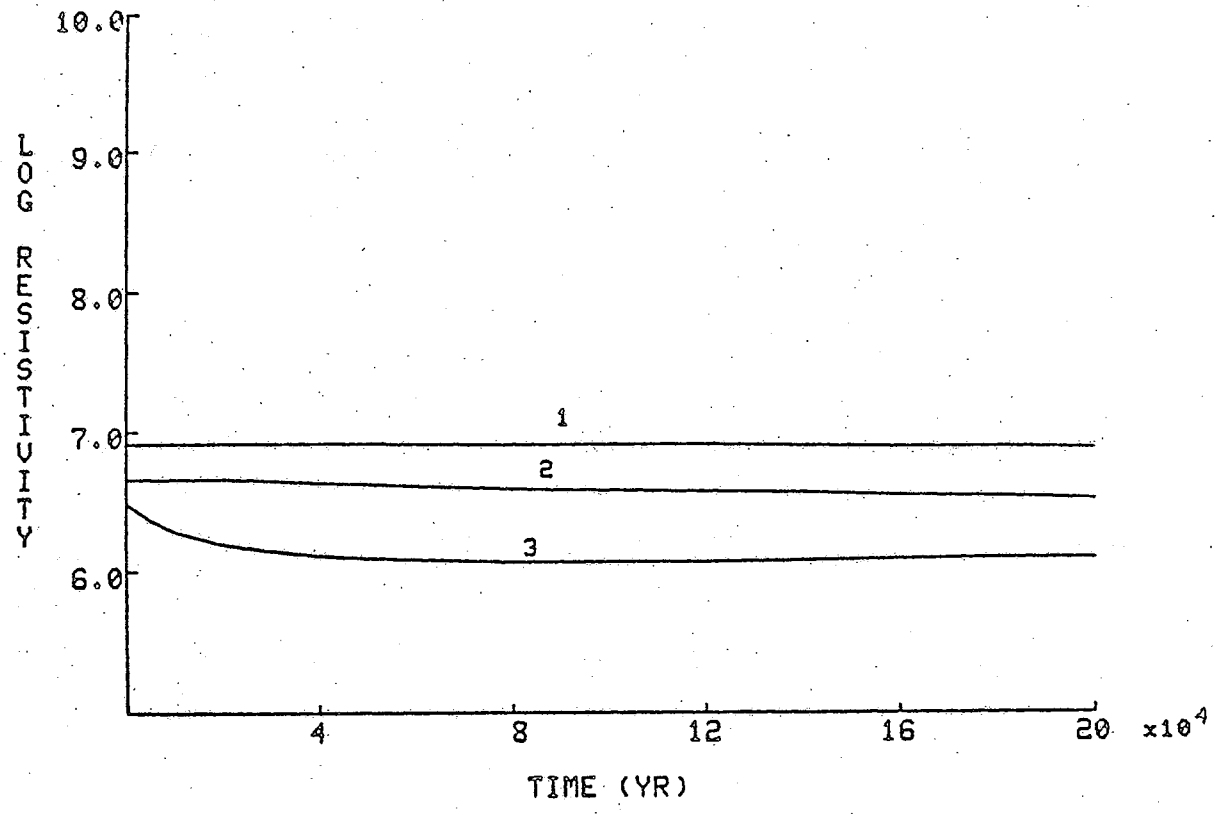

Figure 22. Log Resistivity (ohm-cm) as a Function of Time in Model P1 at Fixed Points 4 km (1), 2.5 km (2), and .5 km (3) Directly above Top of Pluton.

near-surface region. The very small effect of pluton emplacement into impermeable host rocks on near-surface resistivities is the result of slow conductive thermal energy transport away from the pluton.

Convective Model

Model P3 is illustrated in Figure 23 and is characterized by host-rock permeability of 10^{-11} cm^2 and a pluton permeability of 10^{-14} cm^2. The high host-rock permeability in the P3 system allows fluid circulation, and the resultant convective heat transport processes dominate over conductive cooling processes within the host rocks. The low permeability of the pluton results in a conductive cooling of the pluton. The P3 pluton is identical to the P1 pluton with respect to shape and emplacement depth, except that the P3 pluton has a higher initial temperature of 960°C. The initial thermal gradient in the host rocks and the boundary conditions are also identical to those in model P1. The only major difference between these two models is the higher host-rock permeability of 10^{-11} cm^2 in P3 as compared to 10^{-17} cm^2 in P1. The initial and boundary conditions are illustrated in Figure 23. Also shown in Figure 23 are dash lines which denote locations where vertical profiles will be calculated and circles which represent fixed points where the time variation in resistivity and porosity are calculated.

As shown in Figure 24, fluid circulation within the host rocks of the P3 system results in a temperature distribution more convex upward than in the conductive case. As compared to model P1, the isotherms in model P3 are also displaced closer to the top boundary of the system (earth's surface). Also, the isotherms calculated in model P3

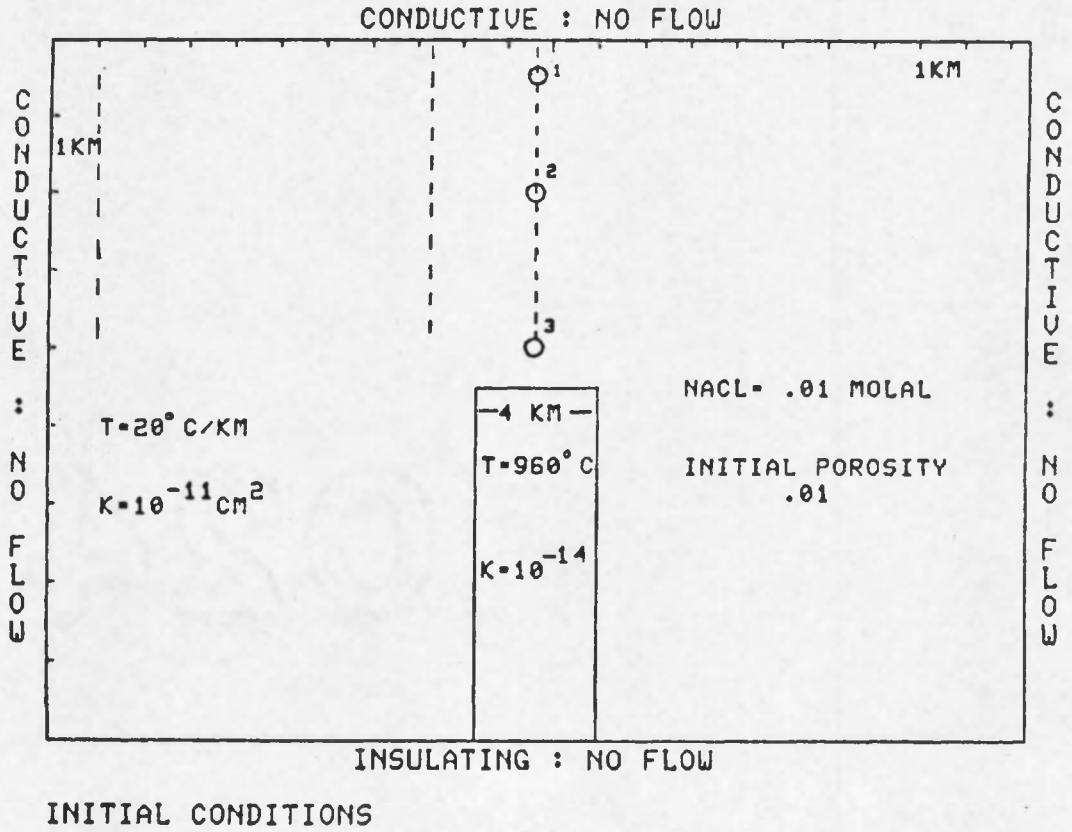

Figure 23. Two-dimensional Cross-section of Model P3 Describing Initial and Boundary Conditions. -- Pluton is shown as rectangular body in center of figure. Dash lines denote locations where vertical profiles will be calculated and circles represent fixed points where the time variation in porosity and resistivity will be calculated. Also shown are K, permeability, T = 20°C/km, initial thermal gradient and T = 960°C, initial pluton temperature. The origin corresponds to upper left hand corner. The top boundary is taken as the earth's surface. The model is symmetric about the pluton's midpoint in the horizontal direction.

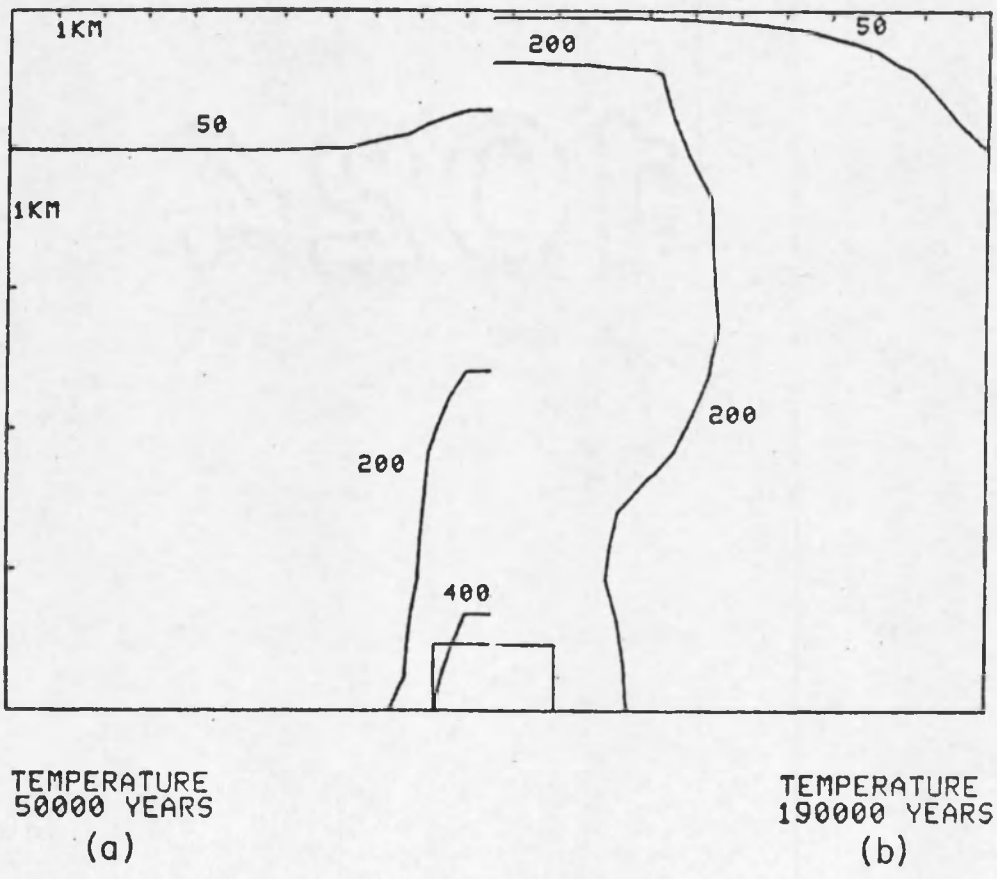

Figure 24. Steady-state Temperature (^{o}C) Distribution at (a) 50,000 Years and (b) 190,000 Years in Model P3.

are displaced inward toward the side contacts of the pluton with respect to isotherms in model P1 at comparable times. The fluid flux within the host rocks contributes to the plumose distribution of isotherms observed at 190,000 years after pluton emplacement (Figure 24b). This results in regions of uniform temperature which are much broader than the thermal source (Norton and Knight, in press). At 190,000 years, the 200°C isotherm in model P3 is at approximately .5 km depth, as compared to 3.5 km depth in the conductive case. The same relationships between the temperature distribution and the porosity maxima and pore-fluid resistivity minima observed in the P1 model will also exist in the P3 system. However, the anomalous region between the 200°C isotherm and the top of the P3 pluton extends from .5 km to 4.5 km depth, as compared to 3.5 km to 4.5 km depth in model P1. Therefore, the maximum increase in initial temperatures occurs directly over the pluton at depths <2 km, as evidenced by the location of the 200°C isotherm in Figure 24b. Also, constant temperatures between .5 km and the top of the P3 pluton will result in constant pore-fluid resistivity and constant porosity between these depths. Before examining the host-rock resistivity distribution in the P3 model, the porosity variation in model P3 will be presented.

The porosity variation with depth is shown in Figures 25 and 26. The vertical lines along which these depth profiles were calculated are shown in Figure 23. The porosity variation with depth at 50,000 years (Figure 25) is comparable to the porosity variation in model P1. However, in model P3 the porosity increases are slightly larger and occur at shallower depths than in model P1. At 190,000 years after pluton emplacement (Figure 26), porosities in host rocks at depths <2 km

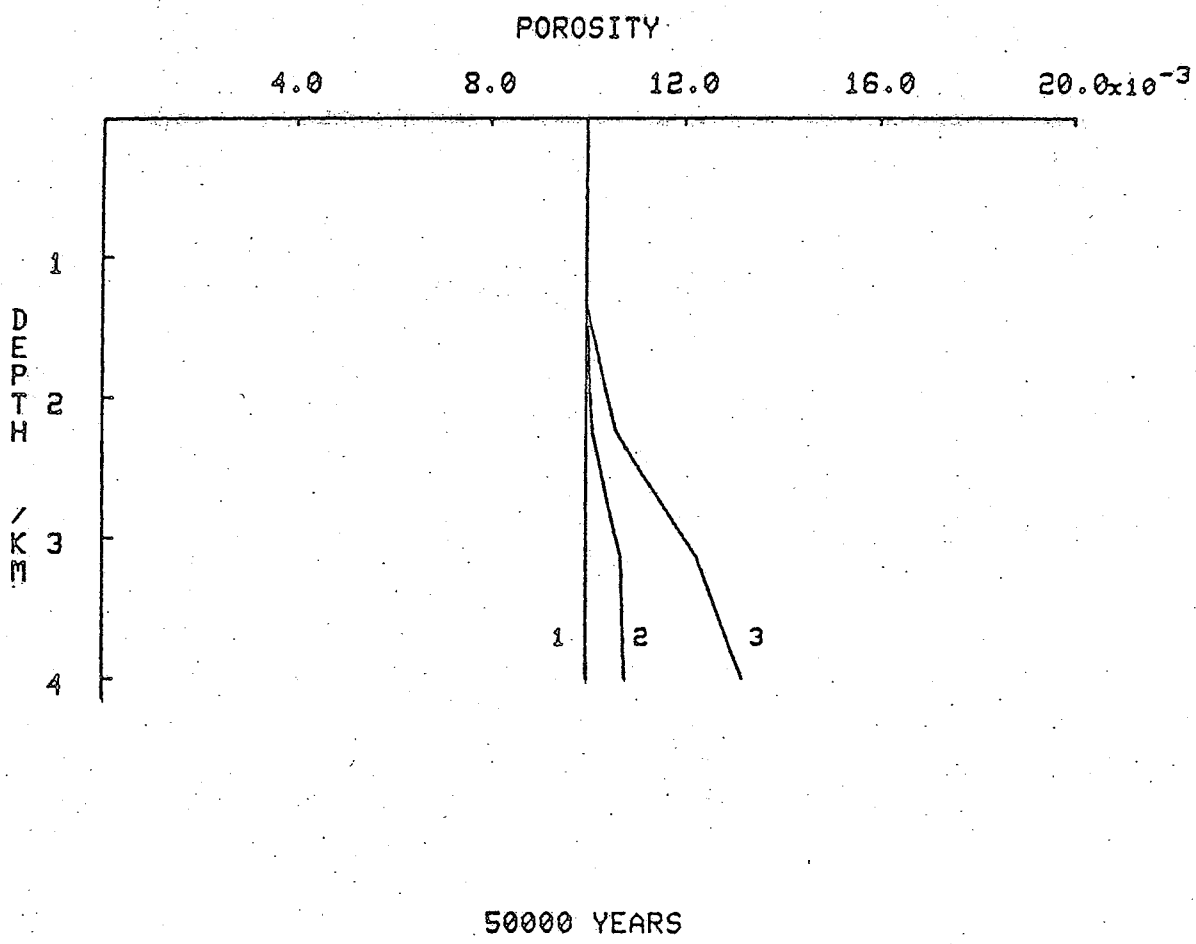

Figure 25. Vertical Porosity Gradients in Model P3 at 50,000 Years. -- Locations of vertical profiles are 8.5 km (1) and 1 km (2) from side contact of pluton and through center (3) of pluton.

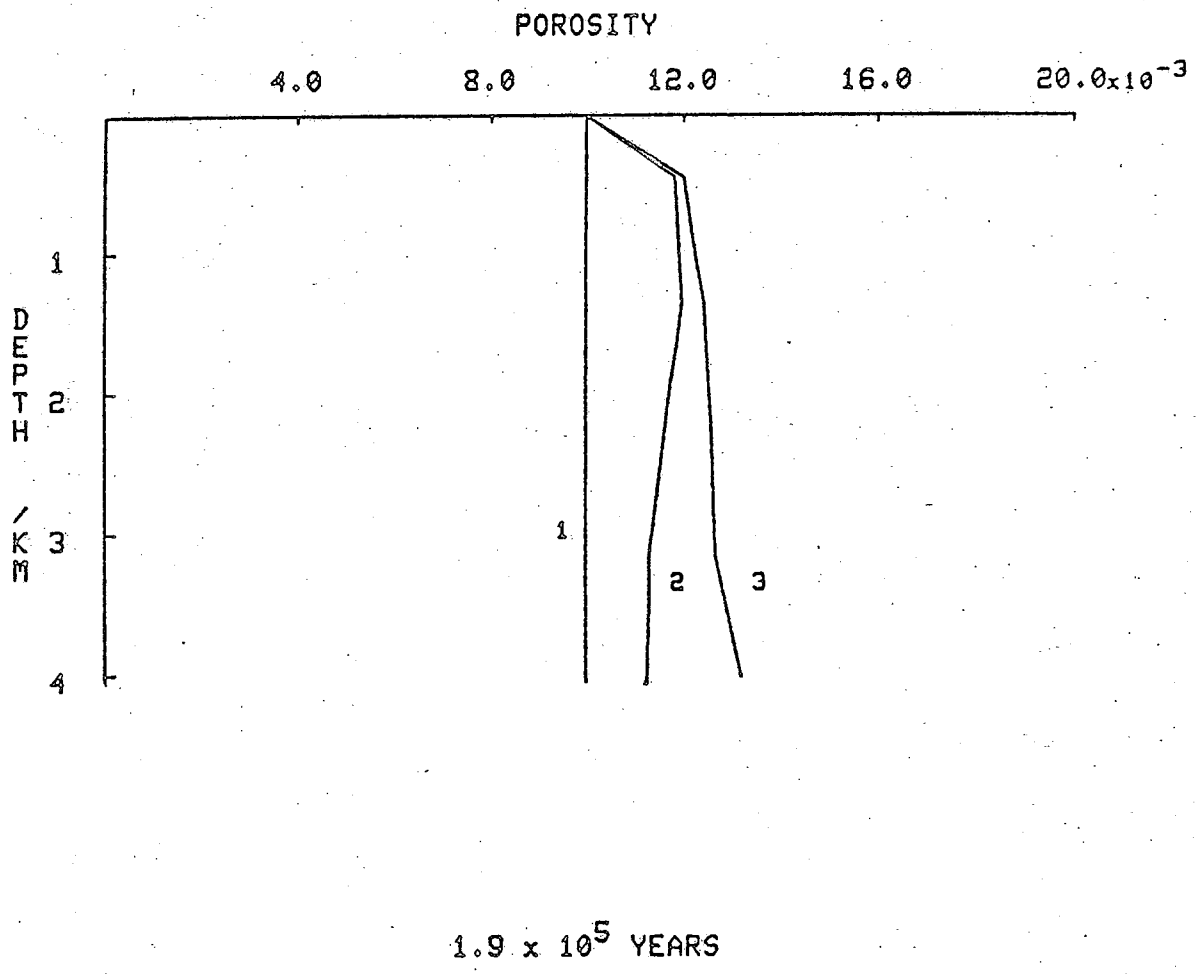

Figure 26. Vertical Porosity Gradients in Model P3 at 190,000 Years. -- Locations of vertical profiles are the same as in Figure 25.

directly over the pluton (curve 3) have significantly increased. This porosity increase is approximately 20% from initial values and persists uniformly to 4 km depth. The porosity profile calculated 1 km from the side contact of the pluton (curve 2) follows the same general pattern as the profile calculated directly over the pluton (curve 3). Although the values of the porosity maxima for both the conductive and convective model are similar, the depth at which this maxima is reached is different. The porosity maxima in model P1 was not reached until 4 km depth, whereas the porosity maxima in the P3 model is reached at .5 km, at an elapsed time of 190,000 years. To further contrast the porosity variation between these two models, the time variation in porosity was calculated at fixed points 4, 2.5, and .5 km above the top of the P3 pluton. These points are shown as circles in Figure 23, and the resulting porosity variations are illustrated in Figure 27. It is immediately evident that the time variation in porosity is more complex in the P3 system than in the P1 system. The major contributor to this complexity in porosity is the thermal transportive properties of the circulating fluids. The first porosity maxima occurring .5 km above the P3 pluton (curve 3) is comparable to the porosity maxima calculated above the P1 pluton. The second porosity maxima occurring above the P3 pluton at 100,000 years corresponds to the maxima in the thermal coefficient of expansion (α_f) of the pore fluid between 200°-300°C. At depths <2 km, a 20% increase in porosity occurs at 100,000 years (curves 1 and 2). Following the porosity maxima at 100,000 years, porosity slowly decays at all three points above the pluton until the end of the model at 190,000 years. However, due to the rapid transport of thermal energy to

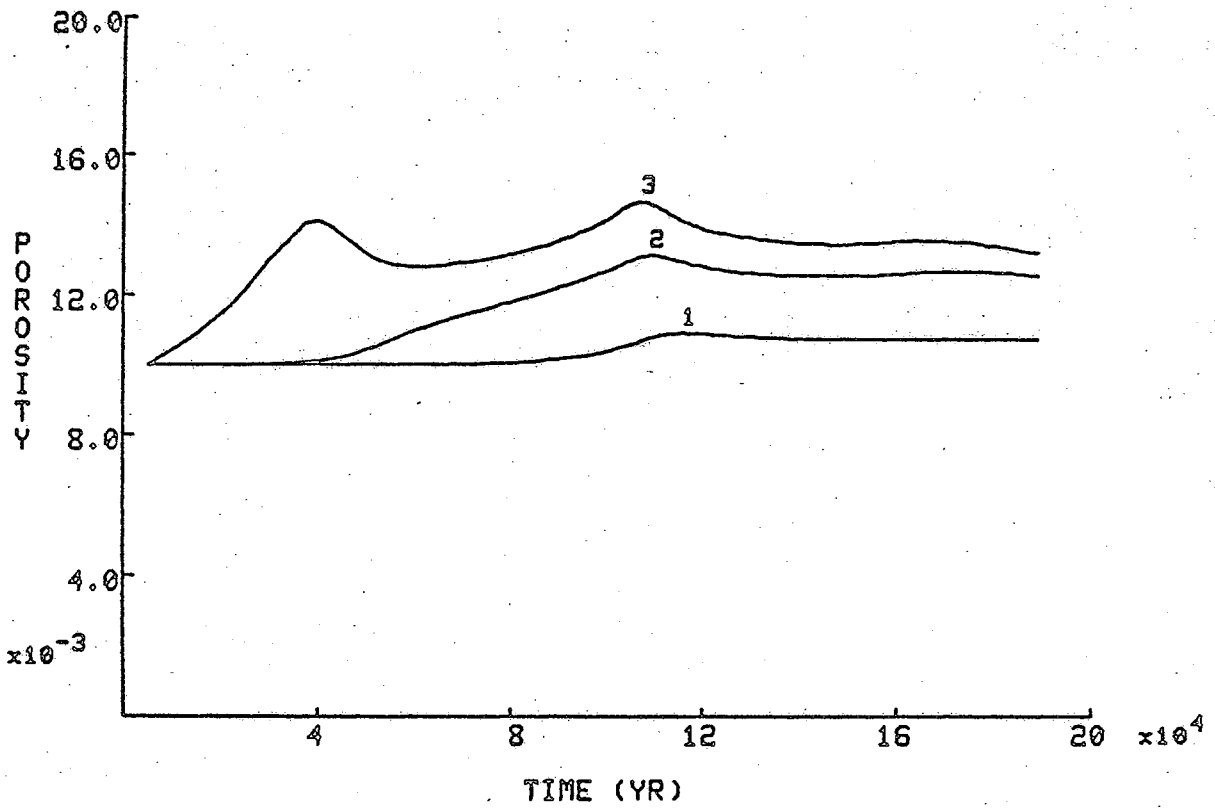

Figure 27. Porosity as a Function of Time in Model P3 at Fixed Points 4 km (1), 2.5 km (2), and .5 km (3) Directly above Pluton.

the surface in model P3, a porosity maxima is observed at depths <2 km. This porosity variation for model P3 is very different from the porosity variations calculated for the conductive case (Figure 16).

The spatial and temporal distribution of temperature in the P3 system will directly determine the host-rock resistivity distribution. Figures 28 and 29 illustrate the resistivity isopleths and isotherms at 50,000 and 190,000 years, respectively. As in the P1 system, the resistivity isopleths parallel the isotherms. However, due to the temperature distribution in the P3 model, a plumose pattern of resistivity is developed by 190,000 years after pluton emplacement. Figure 30 illustrates the displacement in the resistivity isopleths between 50,000 and 190,000 years. By 190,000 years, the lateral extent of the isopleth displacement at 1 km depth spans the entire width of the P3 system (∿22 km).

Resistivity was calculated as a function of depth along lines 1, 2, and 3 of Figure 23, and the resulting resistivity profiles are shown in Figures 31 and 32. The variation in resistivity with depth at 50,000 years is shown in Figure 31. The resistivity gradients at 50,000 years are comparable to those calculated in the P1 model (Figure 20). However, the maximum decrease in resistivity occurs directly over the pluton at a depth of 3 km. The resistivity gradients calculated for the P3 model are coincident until approximately 1 km depth, as compared to 1.5 km in the P1 model. The maximum disparity between the conductive and convective models occurs at 190,000 years (Figure 31). The maximum decrease in resistivity occurs at .5 km depth for the profile directly over the pluton (curve 3) and for the profile at 1 km from the side

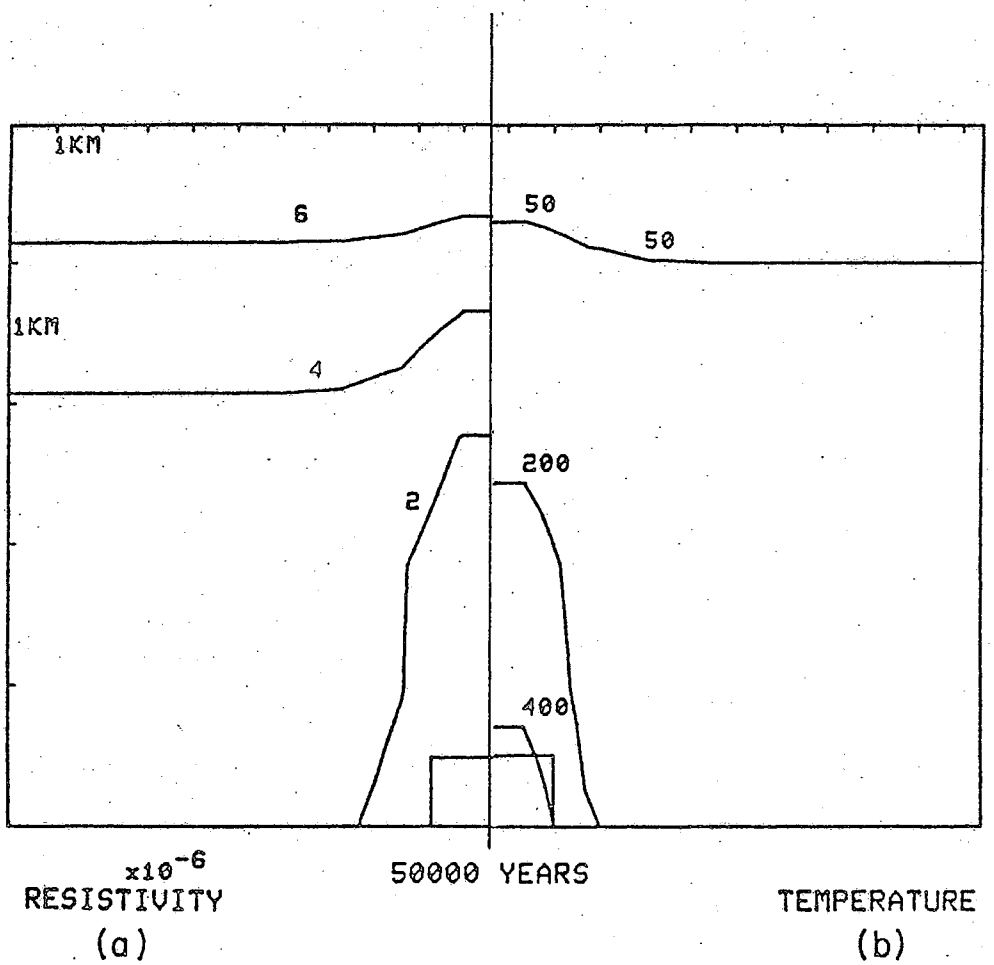

Figure 28. Steady-state (a) Resistivity Distribution (ohm-cm) and (b) Temperature (^{o}C) Distribution in Host Rocks of Model P3 at 50,000 Years.

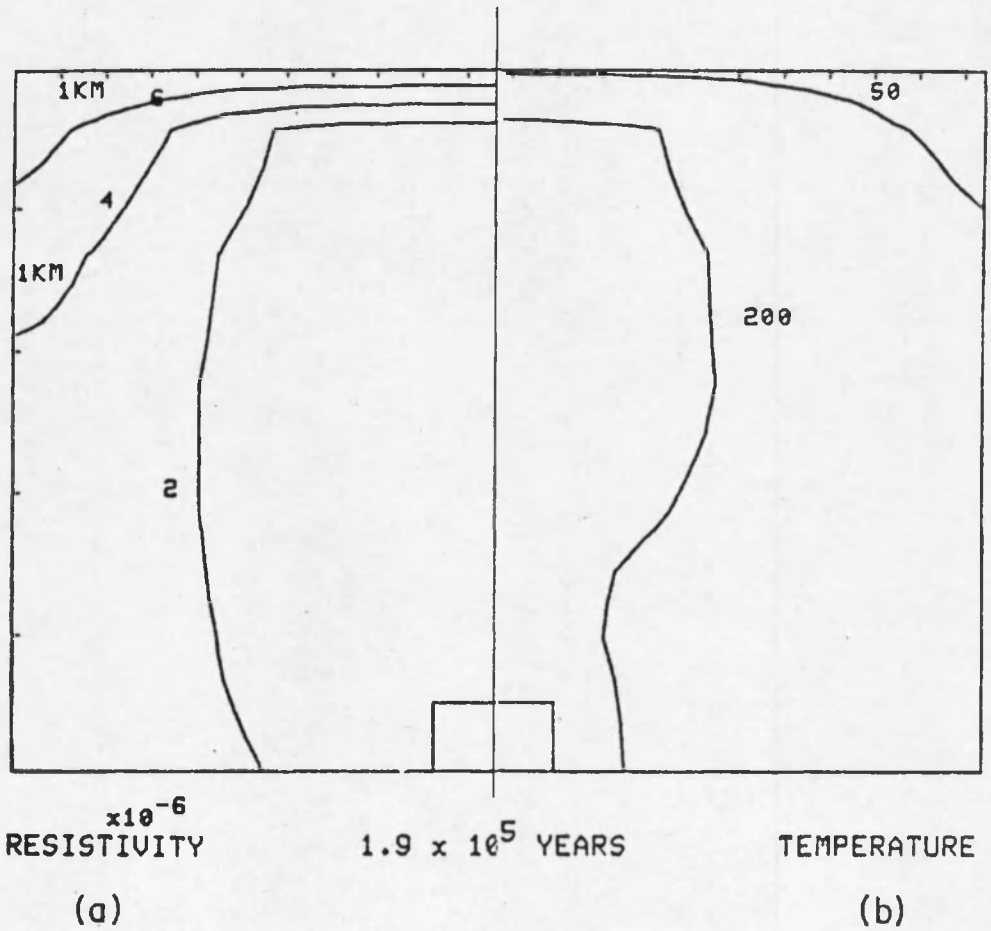

Figure 29. Steady-state (a) Resistivity Distribution (ohm-cm) and (b) Temperature (^{o}C) Distribution in Host Rocks of Model P3 at 190,000 Years.

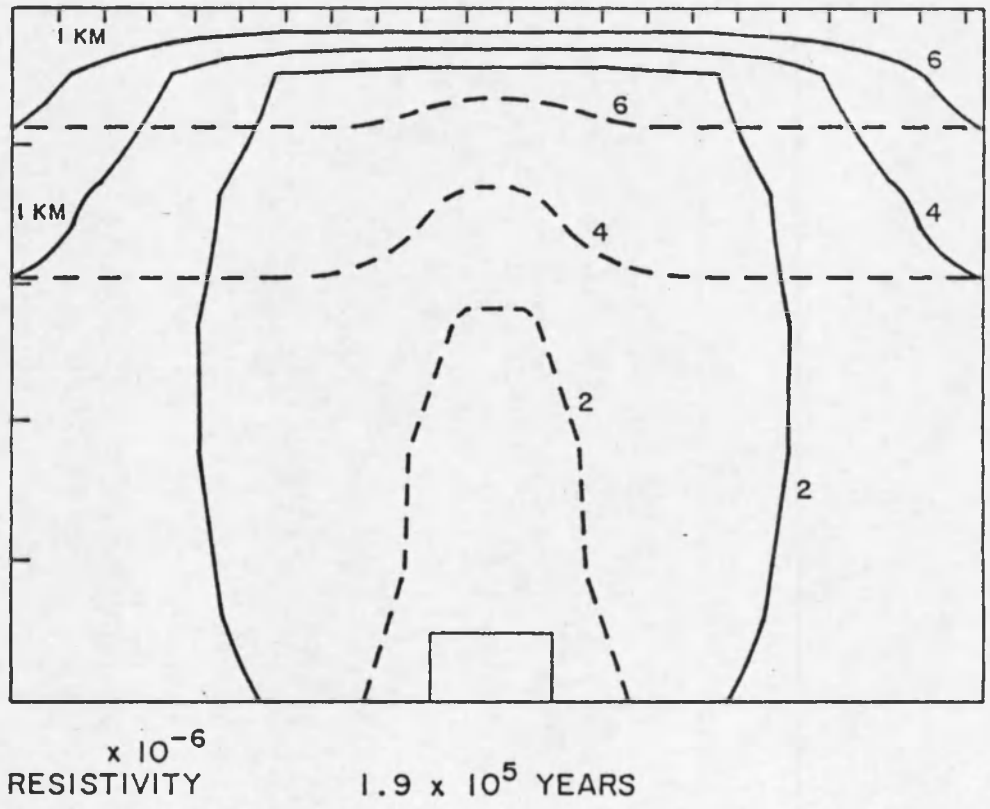

Figure 30. Displacement of Resistivity Isopleths in Model P3 between 50,000 Years (Dash Lines) and 190,000 Years (Solid Lines).

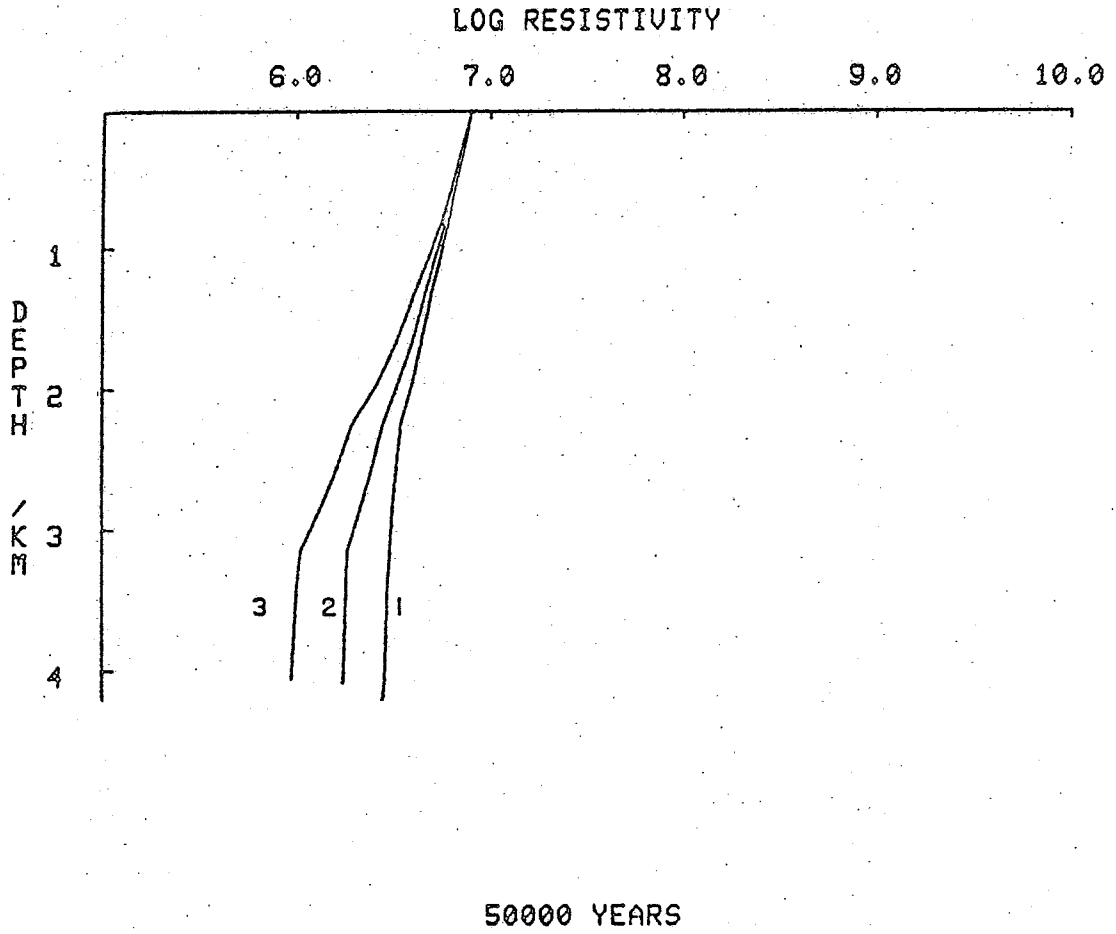

Figure 31. Resistivity (ohm-cm) as a Function of Depth in Model P3 at 50,000 Years. -- Locations of vertical profiles are the same as in Figure 25.

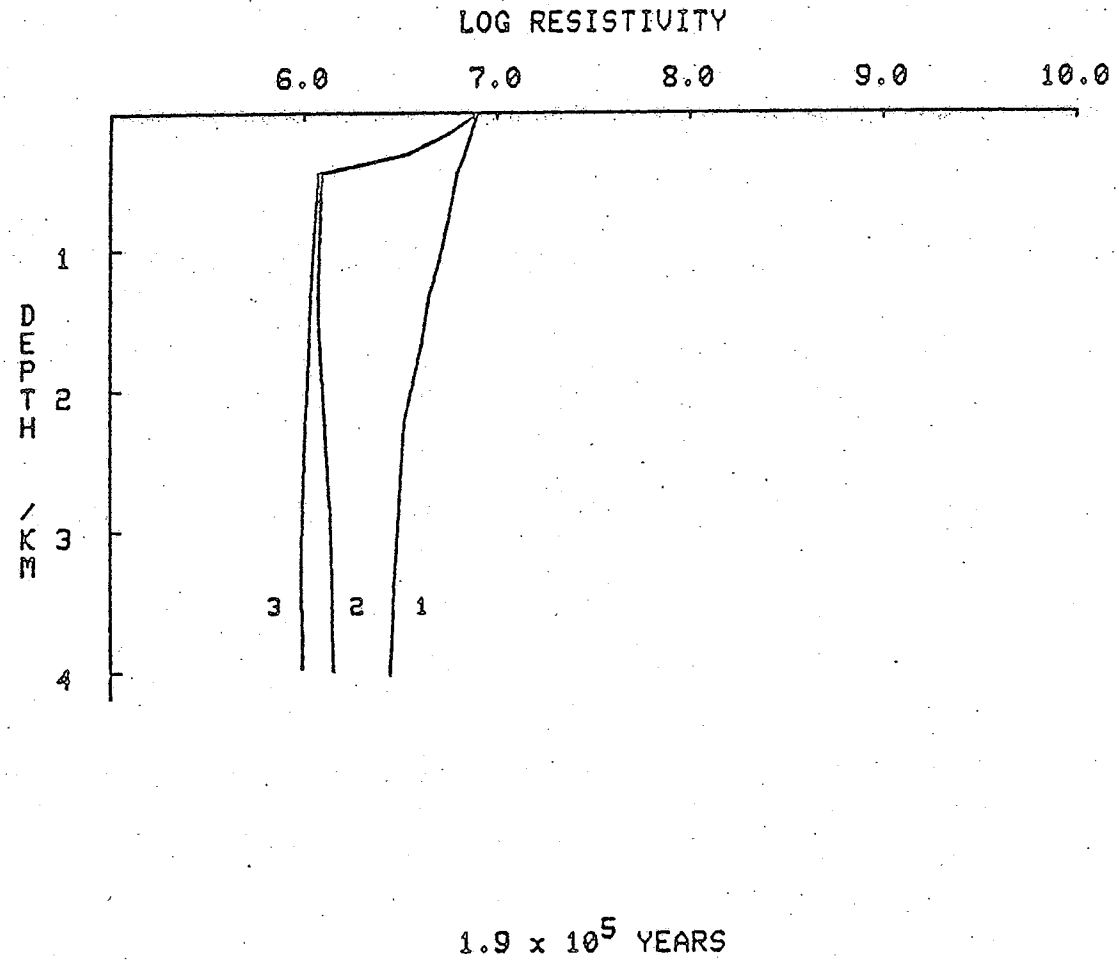

Figure 32. Resistivity (ohm-cm) as a Function of Depth in Model P3 at 190,000 Years. -- Locations of vertical profiles are the same as in Figure 25.

contact of the pluton (curve 2). At depths between .5 km and 4 km resistivity is nearly constant within the host rocks around the P3 pluton. This zone of constant low resistivity is coincident with the zone of constant maximum porosity and constant temperature (200°C) around the pluton (Norton and Knight, in press). Although the maximum decrease in host-rock resistivity (10 fold) and the range in host-rock resistivity (10^6-10^7 ohm-cm) for the P3 model are identical to the calculated values in model P1, the spatial distributions of the resistivity minima in the two models are very different.

The time variation of resistivity is shown in Figure 33 for fixed points 4, 2.5, and .5 km above the top of the P3 pluton. The time variation of resistivity is directly affected by the porosity, temperature, and pore-fluid resistivity changes occurring over the pluton. At .5 km above the pluton (curve 3) a resistivity minima occurs at 20,000 years. This minima is analogous to the resistivity minima at 40,000 years, calculated at the same depth in model P1. The shorter time duration required to attain this minima in the P3 system is due to the higher emplacement temperature of the P3 pluton, as well as the faster transport of thermal energy by convection above the pluton. At 100,000 years the decrease in resistivity at point 2 (curve 2) exceeds the resistivity decrease at point 3 (curve 3), resulting from the rapid increase in porosity at point 2 (Figure 24) as compared to the smaller increase in porosity between the two porosity maximas at point 3 (Figure 24). However, by 110,000 years, the resistivities calculated at points 2 and 3 are nearly equal, and this equality represents the zone of constant resistivity above the P3 pluton (Figure 24a). The convective

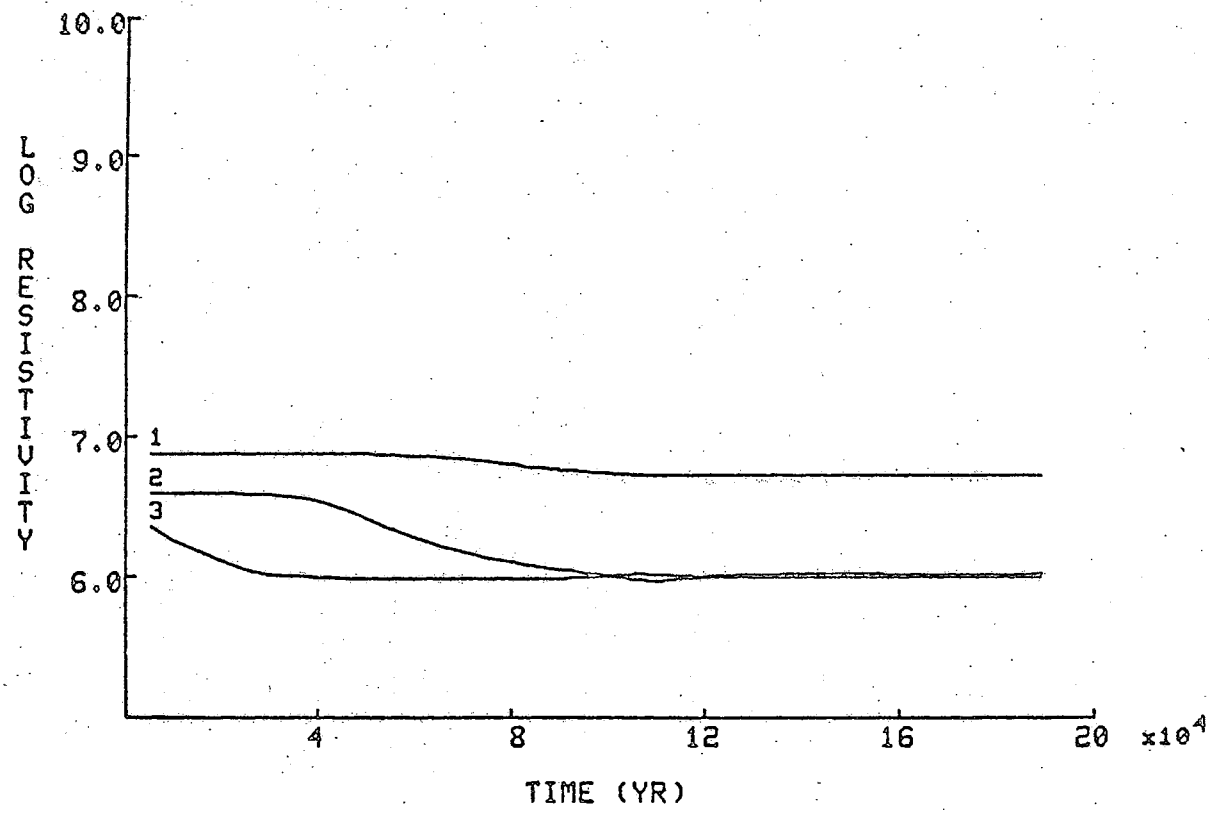

Figure 33. Log Resistivity (ohm-cm) as a Function of Time at Fixed Points 4 km (1), 2.5 km (2), and .5 km (3) Directly above Pluton.

transport of thermal energy away from the P3 pluton results in an order of magnitude decrease in resistivity at depths <2 km by 100,000 years after pluton emplacement.

In summary, the calculations indicate that the dispersion of thermal energy away from a pluton will directly affect fluid resistivities, and host-rock porosities and resistivities. When plutons cool in impermeable host rocks, resistivity variation at depths <2 km is barely discernible by 200,000 years after pluton emplacement. However, when fluid circulation within the host rocks becomes the dominant agent of thermal energy transport, significant decreases in resistivity at depths <.5 km are calculated. This decrease in resistivity persists uniformly in a vertical zone, extending from .5 km to approximately 4 km above the pluton by 190,000 years after pluton emplacement. In both models, the maximum decrease in resistivity does not exceed a factor of 10, as compared to surface values. Also, the range in host-rock resistivity for both models is from 10^6-10^7 ohm-cm.

DISCUSSION AND CONCLUSIONS

Two heuristic models, P1 and P3, have been analyzed with respect to the evolution of fluid resistivity and host-rock porosities and resistivities caused by an igneous thermal source at shallow crustal depths. The results of these calculations include two major conclusions:

1) Except in anomalously high salinity and high porosity environments, the influence of hot circulating saline fluids alone is not sufficient to generate the low resistivity values observed in geothermal areas.
2) The combination of high near-surface thermal gradients, low resistivity anomalies, and surface thermal affects do not assure the existence of a high energy geothermal source at depth.

These concluding remarks will first discuss the effect which varying salinity and porosity have on the magnitude of host-rock resistivities (ρ_R). Second, hypothetical examples will be discussed which show how erroneous conclusions may be obtained by interpreting low resistivity and high heat flux as diagnostic features of high energy geothermal sources.

The range in magnitude for ρ_R in both computer models P1 and P3 is identical. However, the resistivity distribution for these two models is very different. This difference in resistivity distribution is the result of the different thermal regimes in the models. The magnitude of ρ_R is determined by the pore-fluid resistivity and initial host-rock

porosity, while the temperature distribution determines the distribution of ρ_R. To determine the change in magnitude of $_R$, due to varying pore-fluid salinity and host-rock porosities, a series of computer models were calculated with different initial values of porosity and pore-fluid salinity. This series of computer models will be used as a basis for analyzing resistivity in four geologic environments: (1) sedimentary basins, (2) old geothermal systems, (3) young geothermal systems, and (4) mature geothermal systems.

Two concentrations of NaCl, .01 and .1 molal and two initial porosities, .01 and .1, were used to generate four different computer models. Each model used the thermal regime of model P1. The results of these computations are shown in Table 4 and are displayed graphically in Figure 34. The curves illustrated in Figure 34 are an idealized order of magnitude approximation to the actual effects which salinity and porosity have on bulk-rock resistivity. Two assumptions have been used in generating the curves in Figure 34:

1) On an order of magnitude basis, the following relationship exists between water resistivity and NaCl concentration in the temperature range 100^{o}-300^{o}C and pressure range 1 to 1000 bars:

$$\rho_w(\text{ohm-meters}) = {}^{1}/(\text{molality of NaCl}) \qquad (43)$$

2) Concentration of NaCl varies linearly with water resistivity over the temperature and pressure range defined in 1).

Table 4. Results of Varying Salinity and Porosity in Model P1.

Initial Porosity	NaCl Concentration (molal)	$\rho_{R_{min}} < \rho_R < \rho_{R_{max}}$ (ohm-m)
.1	.1	$10 < \rho_R < 100$
.1	.01	$10^3 < \rho_R < 10^4$
.01	.1	$10^2 < \rho_R < 10^3$
.01	.01	$10^4 < \rho_R < 10^5$

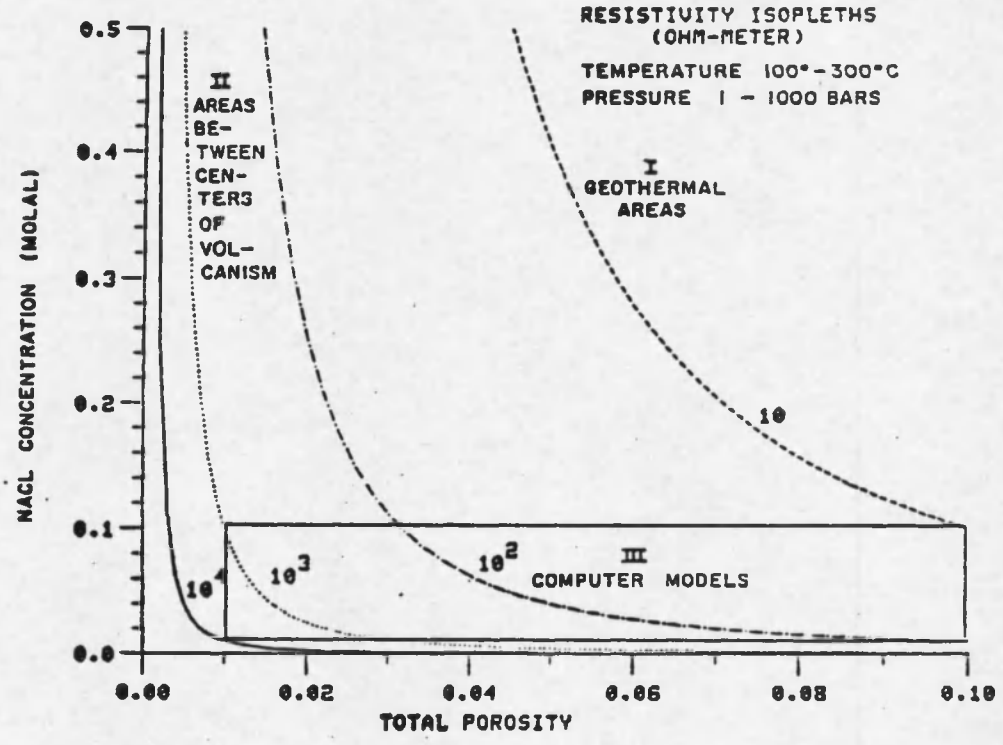

Figure 34. An Order of Magnitude Approximation to the Actual Effects which Salinity and Porosity May Have on Bulk-rock Resistivity.

Using Archie's Law, salinity and porosity were varied in such a way as to keep the bulk-rock resistivity constant, thereby producing the resistivity isopleths in Figure 34. As indicated by the 10 ohm-m curve, high salinity and/or high porosity is required to maintain a resistivity value of 10 ohm-m. Also shown in Figure 34 are three areas corresponding to (1) geothermal areas, (2) crustal areas away from active centers of volcanism, and (3) computer models P1 and P3. The relative positions of areas 1 and 2 are based on results from resistivity surveys in geothermal areas and resistivity surveys in areas removed from active centers of volcanism. It must be remembered that the numerical resistivity models calculated in this study are based on the effects which circulating hot saline waters have on intrinsic rock resistivity. As indicated by the model calculations, to produce the observed resistivities in geothermal areas (<10 ohm-m), high salinity pore fluids and/or high porosity host rocks must occur for large vertical and horizontal zones within the geothermal system.

The total dissolved solid content of natural fluids may range from 1 molal observed in the Imperial Valley geothermal area (Meidav and Furgerson, 1972) to .02 molal observed at Broadlands, New Zealand (Browne and Ellis, 1970). Porosities rarely exceed .1 in most geothermal systems. The discrepancies between the numerical resistivity models and field resistivity observations in geothermal systems may be accounted for by the influence of conducting minerals. As discussed previously, sulfide minerals and clay minerals can reduce intrinsic rock resistivity by two to four orders of magnitude. If one uses a conservative estimate

of a factor of 10 decrease in host-rock resistivities resulting from conducting minerals, a geologically reasonable range in porosity and salinity can produce the anomalously low resistivity values observed in geothermal areas. Therefore, except in anomalously high salinity and high porosity environments the influence of hot circulating saline fluid alone is not sufficient to generate the low resistivity values observed in geothermal areas.

Considerable interest has been given to exploration techniques that might be useful in detecting high energy geothermal systems. The two most commonly used techniques measure heat flow and electrical resistivity. High heat flow in combination with anomalously low resistivity data has been used as a justification for drilling of exploratory wells. Therefore, the implications of the model calculations in this study will be analyzed with respect to four different geologic environments. Emphasis will be primarily on the non-uniqueness problem encountered when attempting to correlate high thermal gradients, low near-surface resistivity, and surface thermal effects with high energy geothermal sources at moderate depth. The first environment to be considered is a typical sedimentary basin found in the basin and range province of the western United States. Concentrated brines associated with evaporite deposits in these basins can produce a lateral density gradient which causes fluid circulation. High porosity is also characteristic of the sedimentary fill of these basins. Coupled with the high salinity and high porosity, exothermal hydration reactions are common in these deposits. These hydration reactions can produce a local thermal

anomaly which might be sufficient to cause high surface heat flux and surface thermal springs. This particular environment is inferred in the Safford Basin, southeastern Arizona (Norton, Gerlach, DeCook, and Sumner, 1975). Therefore, the high salinity and high porosity in these sedimentary basins can generate anomalously low near-surface resistivity, while hydration reactions can give rise to abnormally high surface conductive heat flux and surface thermal effects. However, deducing the presence of a high energy, productive geothermal source at depth with these data can lead to erroneous conclusions in this particular environment.

A second example of a geologic environment which can lead to erroneous conclusions about its geothermal productivity is a geothermal system which has almost decayed to the regional background temperatures. This situation could be examined by continuing the computer models beyong 500,000 years. Also, this particular geologic environment is thought to be observed at Marysville, Montana (McSpadden, 1975). In this instance, the last amount of thermal energy from a buried heat source continues to cause near-surface thermal gradients to be high. Conducting minerals will undoubtedly have been formed above the pluton, and thermal springs will still be prevalent on the surface. In this environment low resistivity would be associated with the conducting minerals and in part with the remnant thermal circulating saline fluids. Once again, deducing the presence of a high energy, productive geothermal source at depth with these data would lead to the wrong interpretation.

A similar geologic environment to the decayed geothermal system is a geothermal system in its early stages. Although no observations of

this type of environment are known, inferrences based on the computer models may be used. The transport of thermal energy away from a pluton is rapid with respect to the mass flux to the surface. This means that hot saline fluids will dominate changes in host-rock resistivities because not enough time has elapsed to produce significant quantities of hydrothermal alteration minerals. High heat flux and surface thermal effects will probably be formed relatively early in the life cycle of a geothermal system. However, the associated resistivity anomaly resulting from increased temperatures results in high resistivity values (10^6-10^7 ohm-cm) which are generally unfavorable for detection by surface methods. Therefore, this environment is characterized by high flux, thermal surface effects, but no substantial low resistivity anomaly, even though there is a possibility of high energy source at depth.

The final example is one of an active, mature geothermal system, examples of which are abundant world-wide. High heat flux, thermal surface effects, and observable low resistivities can be associated in this environment with a productive thermal source at depth. However, the low resistivity anomaly is probably caused by the presence of conductive minerals which are coincident with hot thermal fluids. These results are also observed in the decayed geothermal system. One can easily see the non-uniqueness problem, for in one instance a high energy source is present and in the other a very low energy source is present.

The four geologic environments presented serve to illustrate the problems which can be encountered when attempting to interpret near-surface resistivity anomalies. Also, a combination of heat flux

measurements, surface thermal effects, and low resistivity can be characteristic of both productive high energy geothermal systems as well as unproductive, low energy geothermal environments. These observations are also manifested in the fact that electrical methods are used in prospecting for both sulfide mineral deposits and thermal energy.

REFERENCES

Archie, G. E., 1942, The electrical resistivity log as an aid in determining some reservoir characteristics: Trans. AIME, Petrol. Br., v. 146, p. 54-62.

Brace, W. F., 1971, Resistivity of saturated crustal rocks to 40 km based on laboratory studies, in Heacock, J. G., ed., The structure and physical properties of the earth's crust: Am. Geophys. Union Mon. 14, p. 243-257.

Brace, W. F. and Orange, A. S., 1968a, Electrical resistivity changes in saturated rocks during fracture and frictional sliding: Jour. Geophys. Res., v. 73, p. 1433-1445.

_____, 1968b, Further studies of the effect of pressure on electrical resistivity of rocks: Jour. Geophys. Res., v. 70, p. 5669-5678.

Brace, W. F., Orange, A. S., and Madden, T. R., 1965, The effect of pressure on the electrical resistivity of water saturated crystalline rocks: Jour. Geophys. Res., v. 70, p. 5669-5678.

Brace, W. F., Walsh, J. B., and Frangos, W. T., 1968, Permeability of granite under high pressure: Jour. Geophys. Res., v. 73, p. 2225-2236.

Browne, P. R. L. and Ellis, A. J., 1970, The Ohaki-Broadlands hydrothermal area, New Zealand: mineralogy and related geochemistry: Am. Jour. Sci., v. 269, p. 97-131.

Burges, E. A., Latto, B., and Ray, A. K., 1966, New correlations and tables of the coefficient of viscosity of water and steam up to 1000 bar and 1000°C: Int. Jour. Heat and Mass Transf., v. 9, p. 465-480.

Chambers, J. F., 1958, The conductance of concentrated aqueous solutions of potassium iodide at 25°C and of potassium and sodium chlorides at 50°C: Jour. Phys. Chem., v. 62, p. 1136.

Cheng, W. T., 1970, Geophysical exploration in the Tatun volcanic region, Taiwan: Geothermics spec. issue 2, U. N. Symposium on the Development and Utilization of Geothermal Resources, Pisa, v. 2, pt. 1, p. 910-917.

Clark, S. P., Jr., ed., 1966, Handbook of physical constants (rev. ed.): Geol. Soc. America, Mem. 97, New York, 587 p.

Greenberg, R. J. and Brace, W. F., 1969, Archie's law for rocks modeled by simple networks: Jour. Geophys. Res., v. 74, p. 2099-2102.

Grindley, G. W., 1970, Subsurface structures and relation to steam production in the Broadlands geothermal field, New Zealand: Geothermics spec. issue 2, U. N. Symposium on the Development and Utilization of Geothermal Resources, Pisa, v. 2, pt. 1, p. 248-261.

Gunning, H. E. and Gordon, A. R., 1942, The conductance and ionic mobilities for aqueous solutions of potassium and sodium chloride at temperatures from 15°C to 45°C: Jour. Chem. Phys., v. 10, p. 425.

Heacock, J. G., 1971, Intermediate and deep properties of the earth's crust, a possible electromagnetic wave guide, in Heacock, J. G., ed., The structure and physical properties of the earth's crust: Am. Geophys. Union Mon. 14, p. 1-11.

Helgeson, H. C. and Kirkham, D. H., 1974, Theoretical prediction of the thermodynamic behavior of aqueous electrolytes at high pressures and temperatures, I: Am. Jour. Sci., v. 274, p. 1098-1198.

Jackson, D. B., 1966, Deep resistivity probes in the southwestern United States: Geophys., v. 31, p. 1123-1144.

Keenan, J. H., Keyes, F. G., Hill, P. G., and Moore, J. G., 1969, Steam tables: John Wiley and Sons, New York, 162 p.

Keller, G. V., 1971, Electrical studies of the crust and upper mantle, in Heacock, J. G., ed., The structure and physical properties of the earth's crust: Am. Geophys. Union Mon. 14, p. 107-127.

Keller, G. V., Anderson, L. A., and Pritchard, J. I., 1966, Geological survey investigations of the electrical properties of the crust and upper mantle: Geophys., v. 31, p. 1078-1087.

Keller, G. V. and Frischknecht, F. C., 1966, Electrical methods in geophysical prospecting: Pergamon Press, Oxford.

Knapp, R. and Knight, J., in preparation, Decrease in effective pressure by differential thermal expansion of pore fluids: Department of Geosciences, The University of Arizona.

Kramer, J. R., 1969, Subsurface brines and mineral equilibria: Chem. Geol., v. 4, p. 38-50.

Landisman, M., Mueller, S., and Mitchell, B. J., 1971, Review of evidence for velocity inversions in the continental crust, in Heacock, J. G., ed., The structure and physical properties of the earth's crust: Am. Geophys. Union Mon. 14, p. 11-35.

Lindal, B., 1970, The production of chemicals from brine and seawater using geothermal energy: Geothermics spec. issue 2, U. N. Symposium on the Development and Utilization of Geothermal Resources, Pisa, v. 2, pt. 1, p. 910-917.

McSpadden, W. R., 1975, The Marysville Montana geothermal projects final report: Battelle-Pacific Northwest Laboratories, Richland, Washington.

Meidav, T. and Furgerson, R., 1972, Resistivity studies of the Imperial Valley geothermal area, California: Geothermics, v. 1, p. 47-62.

Mitchell, B. J. and Landisman, M., 1971, Geophysical measurements in the southern great plains, in Heacock, J. G., ed., The structure and physical properties of the earth's crust: Am. Geophys. Union Mon. 14, p. 77-95.

Norton, D., Gerlach, T., DeCook, K. J., and Sumner, J. S., 1975, Geothermal water resources in Arizona: feasibility study: Technical Completion Rept., Office of Water Research and Technology, Project A-054-ARIZ.

Norton, D. and Knapp, R., in preparation, Transport phenomena in hydrothermal systems: the nature of porosity: Department of Geosciences, The University of Arizona.

Norton, D. and Knight, J., in press, Transport phenomena in hydrothermal systems: cooling plutons: Am. Jour. Sci.

Parkhomenko, E. I., 1967, Electrical properties of rocks: Keller, G. V., trans. and ed.: Plenum Press, New York, 314 p.

Porath, H., 1971, A review of the evidence on low resistivity layers in the earth's crust, in Heacock, J. G., ed., The structure and physical properties of the earth's crust: Am. Geophys. Union Mon. 14, p. 127-145.

Quist, A. S., Franck, E. U., Jolley, H. R., and Marshall, W. L., 1963, Electrical conductances of aqueous solutions at high temperature and pressure, 1. The conductances of potassium sulfate water solutions from 25°C to 200°C and at pressures to 4000 bars: Jour. Phys. Chem., v. 67, p. 2453-2459.

Quist, A. S. and Marshal, W. L., 1968, Electrical conductances of aqueous sodium chloride solutions from 0°C to 200°C and at pressures to 4000 bars: Jour. Phys. Chem., v. 72, p. 684-703.

Quist, A. S. and Marshal, W. L., 1969, The electrical conductances of some alkali metal halides in aqueous solutions from 0°C to 800°C and at pressures to 4000 bars: Jour. Phys. Chem., v. 73, p. 978-985.

Risk, G. F., MacDonald, W. J., and Dawson, G. B., 1970, D. C. resistivity surveys of the Broadlands geothermal region, New Zealand: Geothermics spec. issue 2, U. N. Symposium on the Dev. and Util. of Geothermal Resources, Pisa, v. 2, pt. 1, p. 287-294.

Sato, K., 1970, The present state of geothermal development in Japan: Geothermics spec. issue 2, U. N. Symposium on the Dev. and Util. of Geothermal Resources, Pisa, v. 2, pt. 1, p. 155-184.

Shankland, T. J. and Waff, H. S., 1974, Conductivity in fluid bearing rocks: Jour. Geophys. Res., v. 79, p. 4863-4868.

Simmons, G. and Nur, A., 1968, Granites: relation of properties in situ to laboratory measurements: Science, v. 162, p. 789-791.

_____, 1969, The effect of saturation on velocity in low porosity rocks: Earth and Planet. Sci. Lett., v. 7, p. 183-193.

Smith, J. H., 1970, Geothermal development in New Zealand: Geothermics spec. issue 2, U. N. Symposium on the Dev. and Util. of Geothermal Resources, Pisa, v. 2, pt. 1, p. 232-247.

Walsh, J. B. and Brace, W. F., 1966, Cracks and pores in rocks: Proc. of the 1st Cong. of the Intern. Society of Rock Mechanics, v. 1, p. 643-646, Lisbon, Portugal.

Ward, S. H. and Fraser, D. C., 1967, Conduction of electricity in rocks, in Mining Geophysics: Soc. Exp. Geophys., p. 197-223.

White, D. E., 1964, Saline waters of sedimentary rocks: Am. Assoc. Petrol. Geol. Bull., v, 48, p. 342-365.

Wong, C. M., 1970, Geothermal energy and desalination: partners in progress: Geothermics spec. issue 2, U. N. Symposium on the Dev. and Util. of Geothermal Resources, Pisa, v. 2, pt. 1, p. 892-895.

Zohdy, A. A., Anderson, L. A., and Muffler, L. J., 1973, Resistivity, self potential and induced polarization surveys of a vapor-dominated geothermal system: Geophys., v. 38, p. 1130-1144.